Emerging Challenges of Microactuators for Nanoscale Positioning, Assembly, and Manipulation

Bijoyraj Sahu

Curtis R. Taylor
e-mail: curtis.taylor@ufl.edu

Department of Mechanical and Aerospace Engineering,
University of Florida,
Gainesville, FL 32611-6300

Kam K. Leang
Department of Mechanical Engineering,
University of Nevada-Reno,
Reno, NV 89557-0312
e-mail: kam@unr.edu

The development of manufacturing tools and processes capable of precisely positioning and manipulating nanoscale components and materials is still in its embryonic stage. Microactuators are emerging as important tools capable of precisely positioning and manipulating nanoscale components and materials. This paper provides a summary of the state-of-the-art in the design, fabrication, and application of microactuators for nanoscale manufacturing and assembly. Key characteristics and design models of electrothermal and electrostatic microactuators are described and compared. Specific design requirements for their functionality at the nanoscale are discussed. The results demonstrate the limitations of existing microactuator designs and key challenges associated with their design, modeling, and performance characterization for nanoscale positioning, assembly, and manipulation. [DOI: 10.1115/1.4001662]

1 Introduction

The development of manufacturing tools and processes capable of precisely positioning and manipulating nanoscale components and materials is still in its embryonic stage. Manufacturing of nanoscale structures, devices, and systems require tools that provide highly repeatable and precisely controlled sensing, assembling, and positioning of matter at the nanoscale.

Microactuators are tools that can precisely position and manipulate nanoscale components and materials. Microactuators are defined herein to be actuators produced via standard microelectromechanical system (MEMS)-based fabrication techniques including surface and bulk micromachining, and other replication techniques [1]. These actuators can perform various operations such as grasping, pushing, pulling, positioning, orienting, and bending with nanometer precision. For example, microactuators have been demonstrated to grasp and bond carbon nanotubes (CNTs) (as small as 1–3 nm in diameter) onto atomic force microscope (AFM) probe tips (tip diameter <10 nm) for high-resolution, high-aspect ratio imaging [2]; to manipulate and handle fragile 300 nm thin transmission electron microscope (TEM) lamella [3]; and to precisely probe and separate biological cells/tissues [4,5]. While these examples demonstrate the potential of microactuators to perform nanomanufacturing tasks, the future need to assemble 3D heterogeneous nanocomponents with a high degree of repeatability, accuracy, thermal stability, reliability, and throughput presents new challenges and requires further advances in research [6].

There are many challenges in the design, fabrication, and performance characterization of microactuators for nanoscale manufacturing. Manipulation at the nanoscale requires positioning accuracy and precision in the sub-1 nm range; thus sensing and control schemes must be implemented that account for disturbances (e.g., hysteresis and thermal drift) and enable high resolution and repetitive positioning [7]. Many bio- and nanomaterials are fragile and prone to damage; thus actuators must be able to regulate applied forces from micronewtons to nanonewtons, which requires high-resolution force sensing and control. To date, there exist very few microactuators with integrated contact detection and force sensing down to nanonewtons [5]. Because of the extremely small size of nanocomponents, gravitational force is negligible and surface and intermolecular forces such as electrostatic, van der Waals, and capillary forces become dominant. Thus, new assembly strategies and ways of interacting with these forces must be carefully considered for high-resolution positioning and repeatability in manipulation. For example, a task such as gripping a part may not require mechanical contact as the attractive van der Waals force may be sufficient to secure it [8]. The surface and intermolecular forces vary significantly with the operating environment and material properties of the contacting surfaces, which makes prediction and modeling to account for these forces difficult. Additionally, even minor deviations in the geometry and/or dimensions of actuators can have huge implications on their performance [9,10]. For example, in-plane stiffness can reduce by a factor of 6 for a microactuator dimension reduced by a factor of 2, and such structural changes are coupled with changes in resonance and vibration response [2].

Heat-transfer mechanics at micro- and nanoscales are significantly different from macroscale such as high spatial gradient and transient effects [11,12]. In addition, limitations on the physical size of the actuator, free space tool path, power requirements, materials, and/or desired mechanical output (e.g., actuator deflection-to-input power ratio) present a large parameter design space. Progress has been made in addressing these issues; however, microactuators have yet to provide in the high degree of repeatability, accuracy, throughput, and robustness required for nanoscale manufacturing.

In light of the above challenges and issues, the purpose of this article is to provide an overview of the state-of-the-art in the design, fabrication, and nanoscale application of microactuators. Key issues and challenges associated with their use for nanoscale positioning, assembly, and manipulation are discussed. The article is organized as follows. In Sec. 2, a brief overview of current and emerging nanoscale applications of microactuators is provided. Section 3 describes the different types of actuation and discusses design considerations for nanoscale applications. Section 4 summarizes the state-of-the-art actuator designs, analysis, modeling, and related challenges. The design principles and parameters affecting actuator performance are briefly discussed. This is fol-

Contributed by the Manufacturing Engineering Division of ASME for publication in the JOURNAL OF MANUFACTURING SCIENCE AND ENGINEERING. Manuscript received August 31, 2009; final manuscript received April 12, 2010; published online June 14, 2010. Assoc. Editor: Kevin W. Lyons.

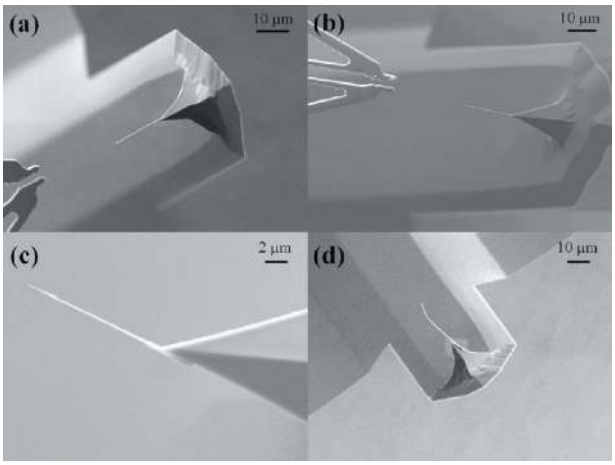

Fig. 1 ((*a*)–(*d*)) Reproducible assembly of CNT-enhanced AFM supertips using topology-optimized microgrippers [2]

lowed by a review of the general fabrication techniques and key issues for microactuators including bulk and surface micromachining techniques in Sec. 5. Finally, Sec. 6 provides an overview of future research directions.

2 Applications

Nanoscale manipulation and assembly are important manufacturing operations for nano- and biotechnology. Microactuators have been shown to be effective at performing a variety of nanomanufacturing tasks including nanometer positioning, picking and placing, patterning, characterizing nanomechanical properties of materials, handling, transport, and assembly of nanoscale objects. In this section, a brief survey is provided, which details nanoscale manufacturing applications of microactuators.

2.1 Nanomechanical Characterization of Nanoscale Thin Films, Tubes, and Wires. Microactuators have been used for nanomechanical characterization of nanoscale thin films, tubes, and wires. Kiuchi et al. [13] fabricated and demonstrated an electrostatic actuated nanotensile test device to measure the fracture stress and elastic modulus of carbon nanowires. The design utilized a comb drive actuator and a cantilever is used to measure applied force. Zhu et al. [14] and Haque et al. [15,16] independently demonstrated thermally and electrostatically actuated devices for nanotensile, bending, and mechanical characterization of nanostructures inside electron microscopes.

2.2 Nanopatterning and Assembly of Nanoscale Parts and Components. Microactuators have demonstrated assembly of nanoscale parts and components. Attachment of a CNT to an AFM tip allows for high-resolution and deep aspect ratio imaging because of the small radius (<2 nm) of CNT tips [17]. Also, soft biological samples can be imaged without damaging the sample as carbon nanotubes are highly deformable. Although methods of growing CNTs directly on AFM tips have been demonstrated, controlling growth at the exact location on the tip is difficult because of the nonplanar tip geometry. However, microactuators have been used to position CNTs directly onto AFM tips for in place bonding, as shown in Fig. 1 [2].

Dip pen nanolithography (DPN) is a technique of forming nanostructures by depositing molecules attached to the tip of a scanning probe microscopy (SPM) probe onto a substrate [18]. Molecules flow to the substrate (see Fig. 2(*a*)) because of the capillary action of the gap between the tip and substrate. By controlling the SPM tip contact with the substrate by means of a bimorph actuator (Au/silicon nitride) [19] or electrostatic actuator [20] discrete patterns with sub-100 nm resolution can be generated [53]. Various polymers, biological compounds, nanoparticles,

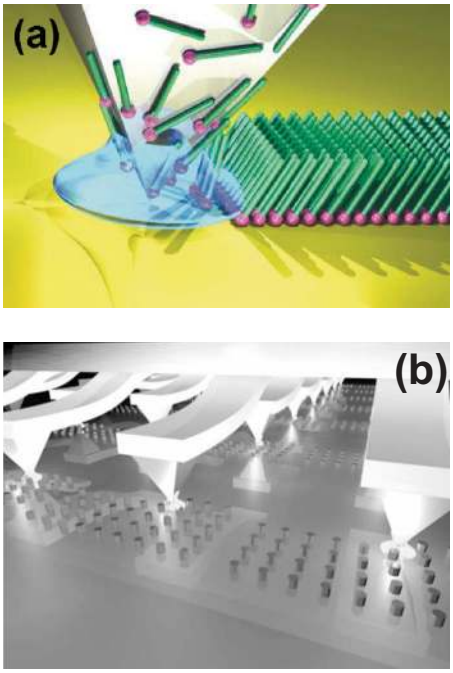

Fig. 2 Dip pen nanolithography showing (*a*) deposition of ink molecules [21] and (*b*) massively parallel (55,000) DPN with 2D cantilever array [25]

metal ions, and sols can be deposited on substrates to create a wide range of nanomaterials [21]. Also, DPN finds potential application for fabrication of biological nanoarrays, which can be used for virus detection and cell isolation. However, practical application requires increased throughput and multifunctionality by parallel arrays of actuators. Bullen et al. [22] demonstrated individual actuation of ten thermal "active" bimorph actuators and thus increasing the parallel writing capabilities. Thermal heating limits application to high melting point ($>62°C$) molecules. Li et al. [23] developed a multifunctional array, which can perform multiple operations of DPN and AFM imaging. Wang et al. [24] developed a thermally actuated multifunctional scanning probe capable of scanning probe lithography (SPL), DPN, and scanning probe contact printing (SPCP) simultaneously. Since the probes were individually actuated, multifunctional operations of patterning and imaging could be performed simultaneously providing for high throughput. Bimorph thermal actuation was used for large actuation, simplicity of fabrication, and low voltage operation. Salaita et al. [25] developed a 55,000 2D cantilever array (see Fig. 2(*b*)) in a cross-sectional area of 1 cm^2.

2.3 Biological and Single Cell Manipulation. The micro-nanoscale size of biological materials and components allows microactuators to play a significant role in the biomedical industry and in future nanoscale biotechnology [26]. Plant and animal cells vary in size from 10–100 μm, bacteria 1–10 μm, viruses 10–100 nm, protein, and DNA 1–10 nm [27]. Cells can be sorted, grasped [4], manipulated, and positioned for cell patterning [28], characterization of structural and functional properties, genetic engineering, drug delivery, DNA injection, and gene therapy. A number of techniques for nanomanipulation of biological samples have been demonstrated including AFM [29], optical tweezers [30], and nanorobots [6]. Microactuators have been used for biological sample manipulation because they are biocompatible, are able to securely grasp and register cells at desired locations, and do so without the bulky equipment or interfering fields associated with optical and electrical manipulation techniques.

Chronis et al. [4] made an electrothermally actuated SU-8 polymer microgripper that successfully gripped and positioned a

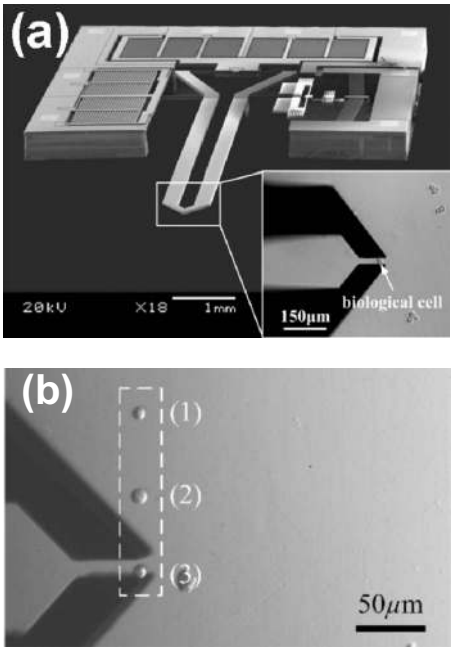

Fig. 3 (*a*) SEM image of silicon microgripper with integrated force sensing and demonstrated control down to 40 nN. (*b*) SEM image of microgripper performing cell transport and alignment [5].

10 μm diameter single cell in aqueous media. The SU-8 polymer allowed for up to 11 μm opening of the gripper for a temperature change of less than 32 °C and an applied voltage of ~2 V. Kim et al. [5] demonstrated force controlled single cell manipulation using a microgripper in aqueous media with force resolution in the nanonewton range. The silicon-based microgripper (Fig. 3) utilizes an electrothermally activated V-beam design for gripper actuation and is integrated with two independent differential capacitive sensors along the in-plane axis (i.e., *x*-*y* axis). Force detection down to ~40 nN was achieved. Microscale magnetic tweezers were shown to maneuver magnetic probes inside living cells with applied forces in the piconewton range [31]. Inoue et al. [32] developed a "microhand" tool for extraction of cytoplasm and mechanical properties measurement of cells using AFM.

Future advances in microactuators will also enable significant breakthroughs in the medical field. For instance, the use of microactuators for minimally invasive surgery will lead to less damage of tissue during delicate surgeries and faster recovery of patients. Feed back control systems will allow precise surgery to be performed at regions not accessible by human hands and existing microtools. In addition, the large-scale microfabrication of low-cost surgical tools can provide health care at an affordable cost.

Table 1 Classification of actuators by type with key characteristics to be considered for nanoscale applications (based on the results of Ref. [34])

Characteristics	Electrothermal	Electrostatic
Force	10 μN–10 mN	10 μN–100 μN
Displacement	Large (20 μm)	Small to large (2–50 μm)
Voltage	Low (0–15 V)	Med. (20–100 V)
Bandwidth	Low (~500 Hz)	High (~kHz)
Footprint (mm^2)	$\ll$1	$>$1

3 Types of Actuation and Capabilities

In this section, we give an overview of the different types of MEMS-based actuation methods. Graphical performance charts developed by Bell et al. [33] provide a quantitative comparison of MEMS-based actuators in terms of maximum force, displacement capability, resolution, and natural frequency. A detailed review of actuators for micro- and nanopositioners can be found in Hubbard et al. [34]. Performance of the actuators is delineated based on range, resolution, footprint, output force, speed of response (bandwidth), and electrical drive considerations. Table 1 summarizes their results in terms of application to nanoscale manipulation. It is worth noting that electrostatic and electrothermal actuators are the most widely used actuators for nanoscale applications. This is because of their straightforward integration with standard MEMS-based fabrication processes, relatively small footprint, and design simplicity. Piezoelectric actuators, on the other hand, are capable of subnanometer positioning resolution and microsecond response times, but are primarily used in the design of nanopositioning stages, in particular, for SPM [7,35]. Progress has been made in development of thin film based piezoactuators [36]; however, issues of residual stress [37], reliability, and lifetime stability require further research. Reviews of piezoactuators across scales are widely available [7,35], thus this article focuses on electrothermal and electrostatic microactuators for nanoscale applications.

3.1 Electrothermal Actuation. Electrothermal actuators operate on the principle of Joule heating and differential thermal expansion [38]. In particular, an electrical closed-loop is formed by designing the actuating mechanism to consist of a *hot* and a *cold* arm. The difference in the heating of each arm induces strain and thus mechanical deformation. The U-beam actuator shown in Fig. 4(*a*) is the most common design [39]. On the other hand, in the bimorph type (Fig. 4(*b*)), mechanical motion is achieved by the differential expansion of two or more dissimilar materials bonded together and having large variation in coefficient of thermal expansion [40]. Typically, electrothermal actuators are suitable for large deflection (up to 20 μm), with output force in the micro- to millinewton range (10 μN–10 mN) and operating voltage well below 15 V. These actuators exhibit the smallest footprints ($\ll$1 mm^2) making them suitable for a wide variety of

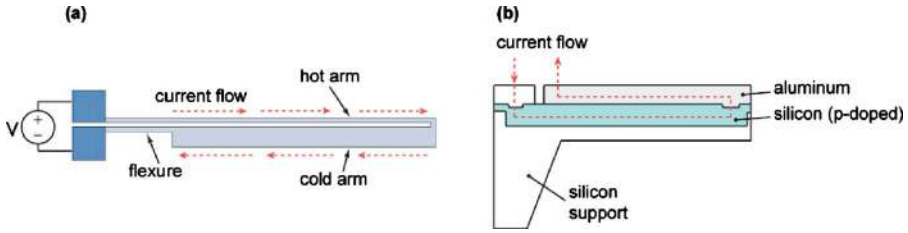

Fig. 4 Schematic diagram of electrothermal actuators showing (*a*) U-beam actuator where higher expansion of the hot arm results in deflection toward cold arm side; (*b*) bimorph actuator that operates on the mismatch of thermal expansion coefficient between aluminum and silicon [40]

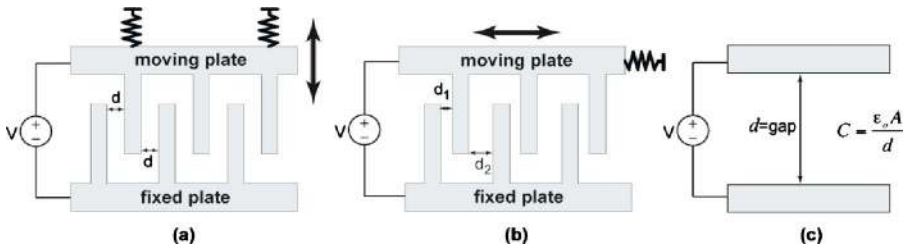

Fig. 5 Schematic diagram of electrostatic actuator showing (*a*) comb drive actuator with perpendicular motion relative to the fixed plate, (*b*) comb drive actuator with parallel motion relative to the fixed plate, and (*c*) parallel-plate capacitor showing change in capacitance as a function of plate area and gap between them [42]

nanoscale applications. However, the high temperature (200–600 °C) may be undesirable for certain temperature sensitive applications. An extensive review of electrothermal actuators can be found in Ref. [41].

3.2 Electrostatic Actuation. Electrostatic actuators operate on the principle of Coulomb attraction due to the application of a bias voltage between two plates (moving and fixed) [34,41]. Two configurations are shown in Fig. 5. The interdigitated or comb drive arrangement produces parallel (Fig. 5(*a*)) or perpendicular motion (Fig. 5(*b*)) of the moving plate with respect to the fixed plate. For the simplest parallel-plate configuration (Fig. 5(*c*)), the capacitance C gives a measure of the stored energy, which is a function of the plate area A, permittivity of the medium ε_o, and distance between the plates d. In general, the output force is a nonlinear function of the gap between the plates. The operating voltage ranges from 20 V to 100 V. Electrostatic microactuators provide higher positioning resolution (<1.5 nm) and faster response (microsecond range) as compared with electrothermal actuators. Because of their straightforward fabrication, small footprint (~ 1 mm^2), and low power consumption, they find potential use at the nanoscale. However, they are not preferable for in situ manipulation in electron microscopes as electric fields due to high voltage may interfere with the imaging electron beam.

3.3 Basic Design Considerations. The design and application of MEMS-based microactuators must take into account size, range of motion, force, resolution, power, dynamic response, reliability, repeatability, environment, and cost.

3.3.1 Size. Small actuator dimensions enable the tool to interact with nanoscale components. For practical considerations, the gap between the arms in a parallel beam is 1–2 μm for effectively manipulating 1D nanomaterials such as alignment of carbon nanotubes on a surface [43]. Bimorph actuators with 400 nm width have been designed [44] and future requirements will extend minimum feature dimensions to the sub-100 nm range. Also, sufficiently small dimensions provide accessibility required for characterization of nanocomponents in scanning and transmission electron microscopes. However, small actuators are also more difficult to handle and interact with from a user point of view.

3.3.2 Range of Motion and Applied Force. Selection of the displacement range and force depends on the type of application. For example, gripping force required for detaching a 50 nm silicon nanowire from a substrate varies from 100 μN to 500 μN, depending on its orientation and position [45]. On the other hand, some applications, such as nanopositioning stages, may require large motion (several micrometers) for assembly operations. Achievable force and displacement depends on stiffness of the geometric structure, which reduces significantly with small dimensions. This necessitates highly optimized geometric design within the small design space.

3.3.3 Actuation Resolution. The resolution of a microactuator is governed by the ability to control the input source affecting actuation and noise level of the supplied voltage/current source. Displacement resolution (~ 0.1 nm/mV) with high precision motion control is required for ultrafine positioning of actuators. Therefore, voltage or current amplifiers must exhibit low noise levels to enable the highest possible actuation resolution. Under feedback control, low noise is advantageous as it maximizes the tracking accuracy [7]. Sensitivity of electrothermal and electrostatic microactuators is a function of position since both have a quadratic relation between voltage and position. Therefore, positioning precision varies with the input voltage/current source.

3.3.4 Contact and Force Sensing. Contact and force detection at subnanonewton levels are imperative to prevent any damage to the fragile actuator and deformable sample. This becomes extremely important in the nanoscale environment where surface and intermolecular forces such as electrostatic, van der Waals, and capillary forces on the order of nanonewtons to micronewtons become dominant [46]. To date, few studies of force sensing methods, such as piezoelectric [47] and capacitive sensing [5], have been explored. Microactuators with integrated high-resolution force sensors will remain a challenge into the near future.

3.3.5 Power. Low power, energy efficient microactuators that operate at lower working temperatures or dissipate less heat have reduced nonlinear effects such as plasticity and drift. Particularly, high peak temperature in electrothermal actuators can induce plastic or viscoelastic response (i.e., for polymers such as SU-8 [48]), which hinders repeatable performance. Designs that minimize power consumption are desirable.

3.3.6 Fabrication and Material Selection. MEMS-based fabrication processes have extended to a wide range of materials. Ashby's methodology for material selection of bimaterial electrothermal [49] and electrostatic actuators [50] provides a very good reference on material selection. For example, in the case of electrostatic actuators, it is suggested that diamond, alumina, silicon, silicon carbide, silicon nitride, and silicon are suitable for high-speed, high-force actuation; polymers for large displacement, low actuation voltage; and aluminum for low resistivity, low-force, high-speed actuation. Thus, design trade-offs must take into account various properties including elastic modulus, electrical resistivity, fatigue strength, density, conductivity, and thermal expansion.

3.3.7 Micro- and Nanoscale Surface Interaction. Surface forces such as adhesion and capillary forces strongly depend on the environmental conditions [51]. An increase in adhesion forces due to humidity may induce stiction of contacting surfaces. Also, temperature fluctuations can change the dielectric properties of piezoelectric actuators. Electrostatic forces may be generated between the substrate/environment at ground potential and charged actuator arm/sample causing loss or damage of the sample. In the

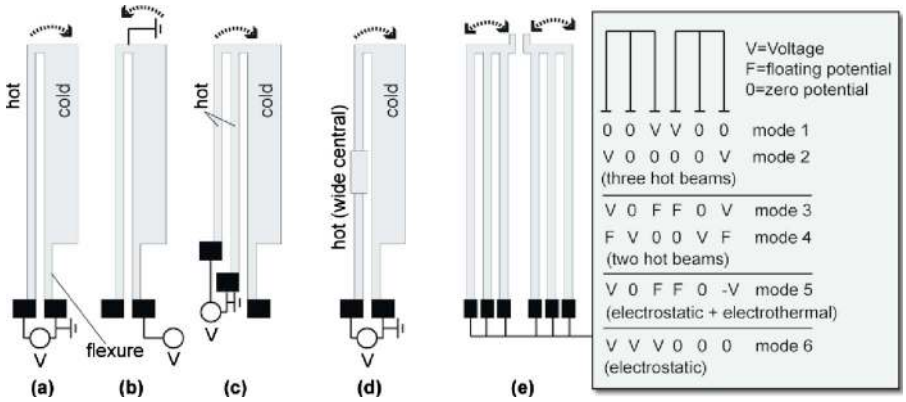

Fig. 6 Top view of U-beam actuators: (*a*) U-beam actuator (in series) where differential expansion of the hot arm results in deflection toward the cold arm, (*b*) U-beam actuator (in parallel) deflection toward hot arm side [62], (*c*) double-U-beam (current path in outer and inner hot arms only) [67], (*d*) hot arm with wide central region for higher deflection and lower peak temperature [64], and (*e*) double-U-beam with uniform hot arms enabling six different modes of operation [43]

case of ionic environments, high voltages (>2 V) will lead to electrolysis [4]. Thus, the environmental conditions and appropriate isolation are critical in the design of microactuators.

3.3.8 Replacement and Cost. Microactuators are fragile due to their small size and would require frequent replacement for practical use in a large-scale manufacturing process. Specific applications would need dedicated actuators and positioners that are low cost and easily replaced, such as the μHexflex ($2 U.S. per device) [52]. Therefore, actuators with simpler design, ease of replacement, and low cost are directly linked to the future affordability of nanocomponents.

In summary, considering the above design requirements, including extremely small forces required for handling nanocomponents, highly complex nanoscale dynamics [53], and small dimensions; a small change in input parameters, material property, boundary conditions, geometrical design, fabricated dimensions, and environment can lead to a drastic variation in operating performance. For example, robust performance (displacement) of the actuator varies significantly ($\sim$50%) with a change in air gap between actuator and substrate from 2 μm to 350 μm [54]. Therefore, microactuators require a systematic design approach with careful consideration of design features and parameters.

4 Design, Modeling, and Analysis

In this section, a review of the state-of-the-art design of microactuators is provided. Various microactuator designs are discussed including U-beam, V-beam, bimorph, compliant mechanism, embedded skeleton-based polymeric actuators, comb drive, and scratch drive actuators. Challenges associated with modeling and analyses are discussed. Finally, experimental methods for performance measurement of microactuators are summarized.

4.1 Microactuator Design

4.1.1 U-Beam Actuator. The conventional electrothermal actuator known as the Guckel, U-beam, or pseudobimorph actuator (Fig. 6(*a*)) consists of a "hot" arm, a "cold" arm, and a flexure [55]. The hot arm is designed with a narrower conductive path than the cold arm, which increases the current density leading to higher Joule heating. This results in differential expansion and in-plane deflection toward the cold arm side. A thin flexure on the cold arm side amplifies the deflection; however, a large reduction in width leads to high temperature. The optimum length of the flexure is within 10–15% of the total arm length [56–59]. Additionally, higher thickness increases out-of-plane stiffness, which is required to prevent unwanted torsion of arms, frequency-dependent cross-coupling effects, and misalignment in operations such as manipulation of a CNT. In the various designs studied [56–59], for geometrical parameters of arm length $l=200-250$ μm, cold arm width $w_c=10-15$ μm, hot arm width $w_h=2-3$ μm, and thickness $h=3-5$ μm, deflection on the order of 15–20 μm could be achieved at voltages less than 10 V and peak temperature within 600°C. Scaling down the actuator dimensions ($l=38$ μm, $w_h=350$ nm, $w_c=1.5$ μm) produced lower but reproducible deflection up to 350 nm for voltages up to 145 mV [60]. U-beam actuators have demonstrated high reliability (3×10^6 cycles within the specified fatigue limit of ±2 μm from equilibrium position [61]). However, the actuator has a single mode of operation, being "open" or "closed," as it deflects toward the cold arm side. Also, high temperature (>200°C) is experienced at the end-effectors that can damage the sample. Another design of the Guckel actuator with current flow in parallel mode is shown in Fig. 6(*b*). It produces deflection toward the hot arm side; however, deflection achieved is less [62]. Furthermore, such an arrangement is not suitable for gripping applications on account of electrical interconnection at the distal end.

Higher deflection can be achieved by adding another hot arm in series with the cold arm, as shown in Fig. 6(*c*) [63]. The current flows only through the hot arms. In this double-U-beam design, the cold arm and flexure are passive elements (no Joule heating) resulting in large temperature differential and higher deflection. Another method demonstrated to increase deflection is by lowering the peak temperature of the hot arm by increasing the width of the central region [64], as shown in Fig. 6(*d*). This improves the deflection by providing a higher power handling capability. Also, deflection can be enhanced by depositing a highly conductive metal thin film on the cold arm [59,65]. This reduces the thermal resistance and increases deflection by approximately 103%. Incorporation of nanoparticles in a nickel actuator has also shown reduced power consumption ($\sim$73%) and increased reliability by improved properties [66].

Tunabilty of open and closed motions can be achieved with uniform width beams as shown by the six different modes of operation in Fig. 6(*e*) [43,47,67]. However, this design provides lower gripping force as compared with the conventional U-beam. Out-of-plane bending may be observed for low aspect ratio (thickness/width) structures. Double-U-beam actuators with geometrical parameters of $l=200$ μm and 100 μm, $w=2$ μm, and $t=2$ and 5 μm could achieve deflection up to 3 μm. Shorter length and higher aspect ratio designs generate large force outputs, but high temperature (>900 K) is required to close the gap.

Out-of-plane U-beam designs [68] are configured with the hot

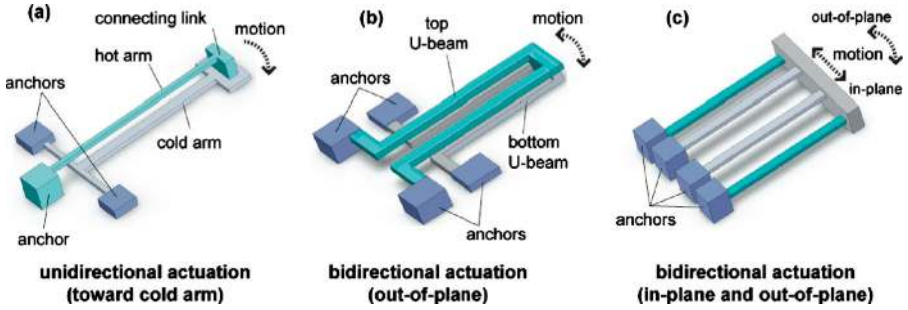

Fig. 7 Schematic diagram of (*a*) out-of-plane unidirectional motion U-beam actuator [69], (*b*) bidirectional U-beam actuator [69], and (*c*) two degree-of-freedom (in-plane and out-of-plane) U-beam actuator [70]

arm positioned above the cold arm, as shown in Fig. 7(*a*). In the bidirectional vertical actuator [69] (BDVA) shown in Fig. 7(*b*), two U-shaped arms (top and bottom) are connected at the free edge. Current flow through the top U-arm produces a vertical deflection toward the bottom arm. Figure 7(*c*) shows a two-degree-of-freedom (DOF) (i.e., horizontal and vertical) design [70]. It is configured with four equispaced parallel hot arms anchored to the substrate at one end and connected to each other by a rigid central shuttle at the other end. The outer and inner arms are at different elevations. By regulating the current flow in the hot arm, the microactuator can deflect in both horizontal and vertical directions. For example, Elbuken et al. [70] demonstrated deflection up to ± 2.4 μm in the horizontal (in-plane) direction and 8.2 μm in the vertical (out-of-plane) direction at an input of 8 V for a 200 μm long actuator.

4.1.2 V-Beam Actuator. The V-beam design is configured with chevron structures placed symmetrically on either side of a movable central shuttle, as shown in Fig. 8(*a*). Joule heating of the chevron structures imparts a rectilinear motion to the shuttle. Motion range of the shuttle can be increased by longer V-beams within thermal buckling limits. The V-beam design provides flexibility in controlling the peak temperature and gripping force by increasing the beam's cross-sectional area. Increasing the number of V-beams can increase the output force. Displacement of the V-beam actuator can be improved by varying the cross-sectional area (contouring) of the hot arm along the actuator length [71]. The contouring provides a more uniform temperature distribution along the length, which can lower power consumption and peak temperature. Also, contouring reduces the thermal errors thereby increasing the actuator accuracy required for nanopositioning applications [71].

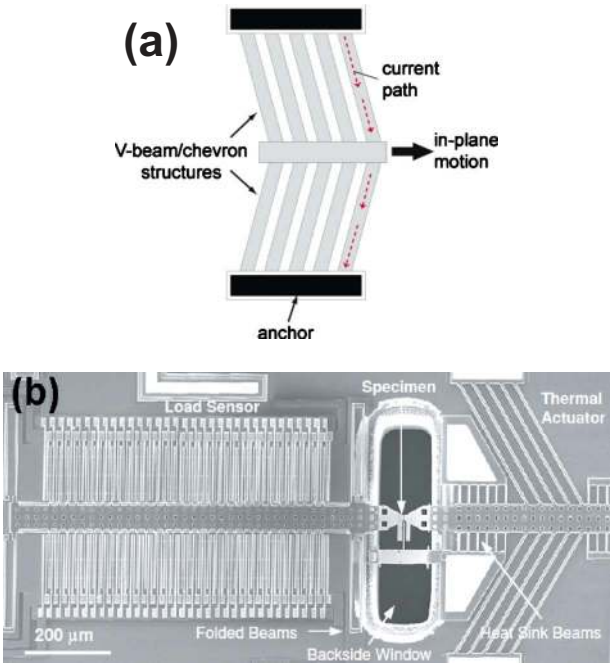

Fig. 8 (*a*) Schematic diagram showing array of chevron structures for the V-beam actuator and (*b*) SEM image of a V-beam actuator used for nanoscale tensile testing with an integrated load sensor [14]

4.1.3 Bimorph Actuator. The bimorph design consists of two or more dissimilar materials bonded together [41,44,72]. Bimorph thermal actuators are advantageous because of their large actuation range ($\sim$50 μm) and low voltage operation. Simplicity of fabrication and large array integration makes them suitable for parallel processing and large throughput applications. For example, 55,000 2D cantilever arrays in a cross-sectional area of 1 cm^2 have been used for DPN [25]. However, the thermal cross-talk, $\sim$23% deflection due to heat transfer from adjacent actuators [20] limits the pitch distance ($\sim$90 μm) between adjacent microactuators. The output force is low as thin bonded materials are required for actuation. Displacement amplification by cascading bimorphs has been reviewed by Geisberger et al. [41]. However, such amplification schemes are not suitable for controlled motion required in nanoscale applications. Also, considering the extremely thin material thickness ($\sim$0.3 μm), it is difficult to integrate sensors required for closed-loop feedback control [73].

4.1.4 Compliant Mechanism. Compliant mechanism based designs transmit motion by elastic deformation of flexible structures [74,75]. In electrothermal compliant mechanisms (ETCs), elastic deformation due to thermal expansion (prismatic joints) provides the actuation force and revolute joints (hinges and flexures) amplify the motion. Moulton and Anathasuresh [62] demonstrated various ETC mechanisms by combination of U-beam actuators for lateral translation and expansion. In their design, the U-beam deflects toward the hot arm side by passing current in parallel configuration (Fig. 6(*b*)). Such an arrangement used in a 3DOF planar micromanipulator is shown in Fig. 9(*a*). Figure 9(*b*) shows the 6DOF μ-hexflexure [52] ETC mechanism with motion ranges of $8.4\times12.8\times8.8$ μm and $19.2\times17.5\times33.2$ mrad, and a displacement resolution of 0.1 nm/mV. The relatively large displacement and high resolution are highly suitable for nanopositioning and manipulation. Tsai et al. [76] made a systematic study and proposed 28 different feasible configurations to transform the conventional rigid links kinematic macromechanism to ETC mechanisms.

ETC designs have been developed by topology optimization [2,77–80]. Topology optimized design uses a finite element based method with a multiparameter optimization algorithm for the op-

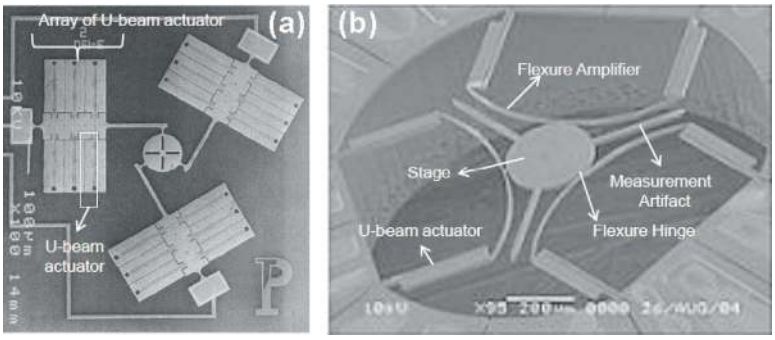

Fig. 9 SEM images of ETC using arrays of U-beam actuators: (*a*) parallel 3DOF planar micromanipulator [62] and (*b*) 6DOF μ-hexflexure nanopositioner [52]

timal material distribution inside a fixed domain. Multiparameter optimization maximizes the deflection for particular design stiffness (rigidity required for stability and gripping force). The distinct advantage of topology optimization is creation of an "active" region and a "passive" region and thus avoids interference of active region current, temperature, and stresses on the sample [80]. The "active region" behaves as the actuating mechanism subjected to high stress and temperature and is close to the anchors. While the "passive region" acts as the compliant mechanism providing range of motion. A topology-optimized electrothermal actuator designed by Sardan et al. [2] (Fig. 10) provides a higher gripping force and lower end-effector temperature within the same geometric domain of the double-U-beam microactuator. Deflection up to 1 μm and gripping force of 18–20 μN were achieved at an end-effector temperature of 229°C.

4.1.5 Embedded Structure-Based Polymeric Electrothermal Actuators. Polymeric electrothermal actuators, usually SU-8 based, provide low handling force, large displacement, and low operating voltages, making them advantageous for handling and manipulation of nanoscale and biological applications [4,82,83]. However, they exhibit slow response because of their lower thermal conductivity. A novel concept of embedding structures within silicon (Fig. 11(*a*)) improves the heat conduction rate providing for uniform distribution [48,84,85]. Also, confinement of the polymer inside the high-aspect ratio silicon structure leads to higher displacement, higher stiffness, and less out-of-plane motion. For example, a silicon skeleton microgripper (440 μm long and 85 μm wide) achieved single arm displacement of 34 μm at an input voltage of 4 V with an average temperature of approximately 170°C [48]. A 2DOF configuration of an embedded structure-based polymeric actuator (17 μm, 196 μN and 11 μm, 814 μN displacement and output force in in-plane x- and y-directions, respectively) is shown in Fig. 11(*b*).

4.1.6 Comb Drive Actuator. Motion of the comb drive actuator is controlled by the equilibrium of the electrostatic force and spring force (spring stiffness in x-direction K_x) of the suspension system. For the parallel motion actuator, electrostatic force in the x-direction (see Fig. 12) is given by Eq. (1),

$$F_x = \frac{n\varepsilon t}{d} V^2 \tag{1}$$

where n is the number of comb pairs, t is the thickness of the plate, d is the gap spacing, ε is the permittivity of the medium, and V is the voltage.

Increasing the number of comb pairs, reducing the gap spacing, and increasing the voltage can increase the force output. Thin fingers with smaller gap spacing increase the power density; however, slender comb fingers may deform individually and contact each other [86]. The gap spacing is also limited due to the pull-in instability condition [87]. Under this condition, the stable displacement occurs for $K_y > K_e$, where K_y is the spring stiffness in the y-direction. K_e is the negative spring constant defined by Hirano et al. [88] as the "derivative of the electrostatic force in y-direction with respect to the spacing between comb fingers in lateral direction" (y-direction) [89]. A modified relation for pull-in instability is developed by Chen et al. [90] that includes a tolerance factor that accounts for minor deviations due to microfabrication and environmental disturbance. In general, under normal conditions the maximum stable displacement $\delta_x^{\max}$ is given by [87]

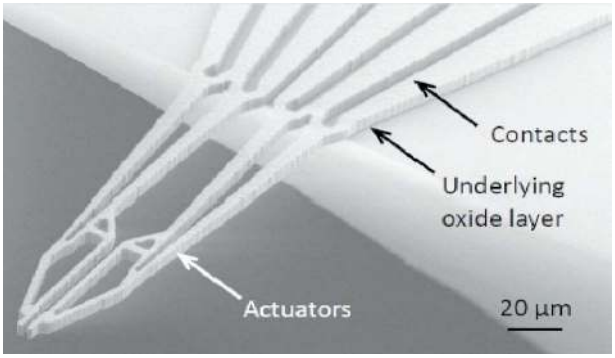

Fig. 10 SEM image of the electrothermal actuator designed by topology optimization, which demonstrated pick and place manipulation of CNTs [81]

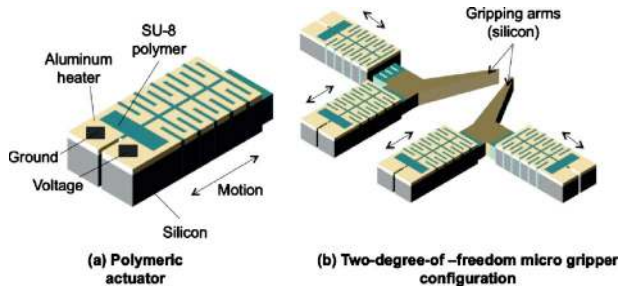

Fig. 11 Schematic diagram of embedded structure-based polymeric actuator. (*a*) Basic configuration consisting of a polymeric expander (SU-8), a meandering shaped skeleton (Si) and thin film heater (Al). (*b*) 2DOF microgripper configuration made of embedded structure-based polymeric actuator [84].

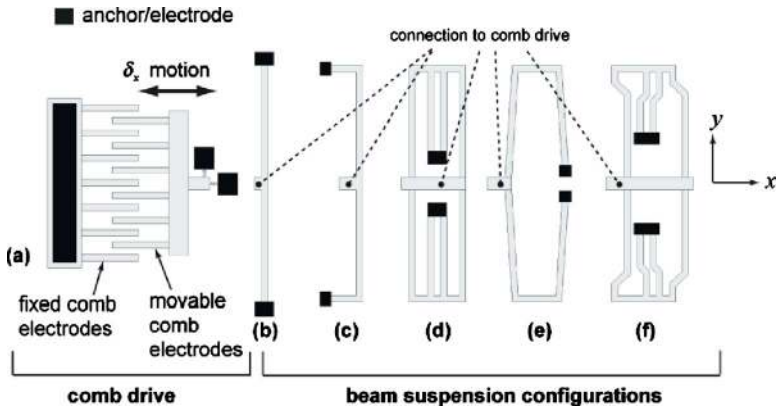

Fig. 12 (*a*) **Schematic diagram of comb drive actuator with different suspension systems:** (*b*) **clamped-clamped beam,** (*c*) **crab-leg beam,** (*d*) **folded-beam,** (*e*) **hybrid spring, and** (*f*) **prebent-tilted beam**

$$\delta_x^{\max} = \frac{1}{2}\sqrt{L_0^2 + \frac{2K_y}{K_x}d^2} - \frac{L_o}{2} \tag{2}$$

which is a function of the spring stiffness in the y-direction K_y, the spring stiffness in the x-direction K_x, the length of overlap L_o, and the gap spacing d between the fixed and movable electrodes. Different methods for increasing the stable displacement as mentioned by Hou et al. [89] include (i) shifting the maximum of suspension system (Fig. 13(*a*)), (ii) negative spring constant reduction (Fig. 13(*b*)), and (iii) minimum of spring constant shifting (Fig. 13(*c*)).

The mechanical design of the suspension system is most important for large displacement comb drive actuators. Since the driving force does not change with motion, linear spring stiffness K_x is desirable for compliance in the x-direction and high stiffness ratio K_y/K_x is required to avoid pull-in instability for large displacement. The clamped-clamped beam (Fig. 12(*b*)) provides a high stiffness ratio K_y/K_x; however, stiffness K_x is linear in the small deflection range only [91]. The crab-leg flexure (Fig. 12(*c*)) improves the linear range of spring stiffness K_x; however, stiffness ratio reduces at higher displacements [91]. The folded-beam design (Fig. 12(*d*)) is better than both the crab-leg and clamped-beam configuration; however, K_y decreases at higher displacement [91,92]. Hybrid spring (Fig. 12(*e*)) with folded-beam [90], tilted folded-beam [87], and prebent-tilted-beam [93] shifts the maximum of spring stiffness K_y and improves the displacement, as shown in Fig. 13(*a*).

Proper design of the comb structure, such as thickness and number of comb pairs (Eq. (1)), improves the force performance of the actuator. Linear variation of the comb finger length, as shown in Fig. 14(*a*), can enhance the displacement by reducing the equivalent electrostatic spring constant (Fig. 13(*b*)) [93]. Methods such as varying gap spacing to obtain linear, quadratic, and cubic electrostatic force curves that vary similarly with restoring spring force ($F=k_1x+k_2x^2+k_3x^3$) also improve the displacement [94]. For example, a two-segment comb structure with two different gap spacings has shown 70% improvement in displacement [95]. Recently, a novel method of cascading three comb drives, as shown in Fig. 14(*b*), demonstrated a 200% increase in displacement [96]. Another method is addition of a secondary comb actuator, as shown in Fig. 14(*c*) [89]. Voltage is initially applied to the primary actuator and shifted to the secondary actuator when it is engaged. This reduces the equivalent electrostatic force (Fig. 13(*c*)) and leads to displacement improvement.

Comb drive actuator arrangement with higher DOF is required for applications like nanopositioning. The common arrangement for bidirectional movement consists of four actuators positioned around a central stage, as shown in Fig. 15(*a*) [95,97–99]. A

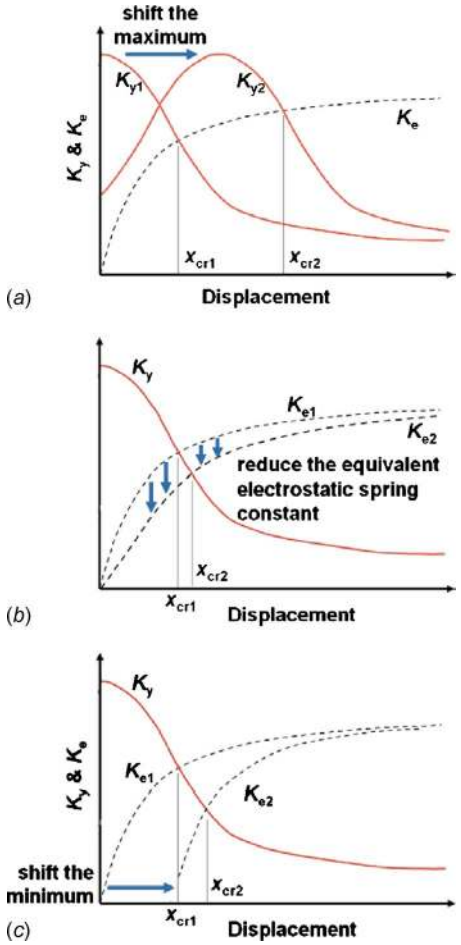

Fig. 13 Methods of improving displacement of comb drives [89]: (*a*) **shifting the maximum of spring stiffness,** (*b*) **reducing the equivalent electrostatic constant, and** (*c*) **minimum of spring constant shifting**

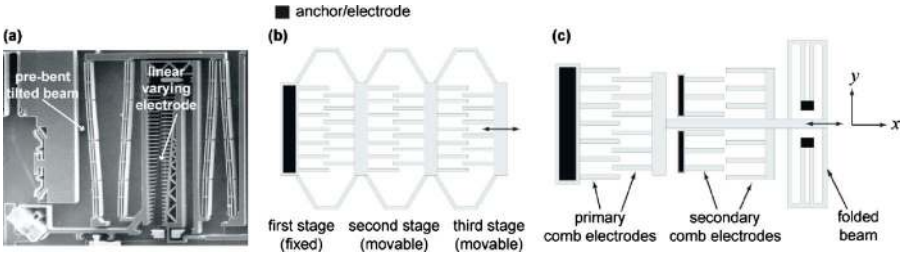

Fig. 14 Comb drive actuators displacement enhancement methods: (*a*) SEM image of linearly engaging teeth and prebent suspension [93], (*b*) schematic diagram of three-stage cascading configuration [96], and (*c*) sequential engagement of primary and secondary comb drives by voltage switching [89]

spring suspension system, usually folded-beam or clamped-clamped beam, provides the restoring force. High lateral stiffness of the suspension system provides decoupling of motion between the orthogonal directions. While reduced stiffness of the tethering-beam connecting the stage to the comb drive allows motion for the orthogonal movement. However, lower stiffness has disadvantages of end-effector rotation, lower resonant frequency, lower bandwidth, and complex dynamics [99]. In serial kinematics mechanism (SKM) design, actuation of one-stage (*x*-direction) is carried within the second stage, which provides actuation in the orthogonal direction (*y*-direction). However, such an arrangement results in a low dynamic response system with additional problems of electrical connectivity [99]. Parallel kinematics mechanisms (PKMs) [99,100] with comb drive actuators and flexure arrangement, as shown in Fig. 15(*b*), provide increased motion range, high structural stiffness, and a balanced mechanical structure [101]. The PKM nanopositioning stage shown in Fig. 15(*b*) achieved translation of 15 μm at 45 V at a natural frequency of 960 Hz. The three-axis nanopositioning [97] shown in Fig. 15(*a*) (in-plane comb drive actuators and out-of-plane parallel-plate actuators) achieved ± 12.5 μm in the *x*- and *y*-directions at 30 V and 3.5 μm in the *z*-direction at 14.8 V. A novel piezoresistive feedback system, essential for closed-loop control, is integrated in the nanopositioning stage developed by Sun et al. [95].

Comb drive actuated manipulators require suitable amplification mechanisms that can convert the micrometer motion into sub-nanometer step displacement with high repeatability and force output [102]. Flexure-based mechanisms that convert the linear motion of the comb drive to rotary motion of the arms for gripping applications suffer from reduced force output due to mechanical conversion and large motion [103]. Combination of linear and vertical comb drive actuators with linear and torsional springs is challenging in terms of fabrication and has limited motion (~ 1 μm) [104]. Comb actuation of a single manipulator arm with integrated capacitive force feedback has demonstrated manipulation of micrometer-scale particles (~ 100 μm) [105]. A nanometer positioning resolution (0.15 nm) comb drive arrangement with a symmetric toggle and lever amplification mechanism and capacitive feedback, as shown in Fig. 16 [102], achieved a motion range of ± 2.55 μm with a force capability of 98 μN.

Another variation of comb drive actuators is the parallel-plate arrangement shown in Fig. 5(*b*). However, in such an arrangement the displacement is limited to one-third of the initial gap (~ 2 μm) due to pull-in instability [106]. Methods for improving the displacement are leveraged beam and stress stiffening [107], folded capacitor method [108], current drive [109], voltage drive [110], and the two-beam method [106].

4.1.7 Scratch Drive Actuator. Scratch drive actuators (SDAs) [111] generate high force (>100 μN), large displacement (~ 100 μm), and nanometer positioning resolution (~ 10 nm) [112]. They can operate over a wide range of speeds (70–250 μm/s dependent on amplitude and frequency of the input signal). Warping motion of the SDA due to electrostatic force imparts motion to the stage, as shown in Fig. 17. However, voltages may be as high as 290 V with motion detection at 60 V in addition to complex circuit design [111]. Also, the upward-downward and impact motion (due to warping) may not be suitable for gripping and precision nanoassembly operations.

4.2 Modeling of Microactuators and Related Challenges. Analytical models provide insight on device performance, and the models can be used to determine the critical design parameters affecting the performance of an actuator. In this section, a brief review of the analytical models and related challenges for microactuators are provided.

4.2.1 Analytical Models. Numerous analytical models have been cited in the literature for the electrothermal in-plane U-beam actuator [56,57,113], out-of-plane U-beam actuator [69,114], and V-beam actuator [71,115]. In general, the solution for temperature distribution is obtained by considering the balance between Joule heating and the three primary modes of heat transfer: conduction,

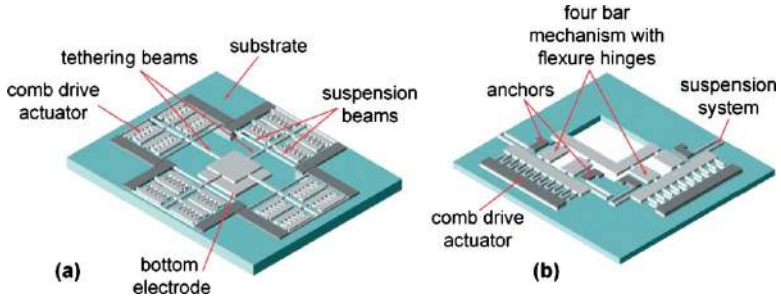

Fig. 15 Schematic diagram of nanopositioning stages with comb drive actuators: (*a*) three-axis MEMS nanopositioning stage with *z*-axis motion by parallel-plate actuator [97] and (*b*) parallel kinematic four bar mechanism with flexure hinge configuration [99]

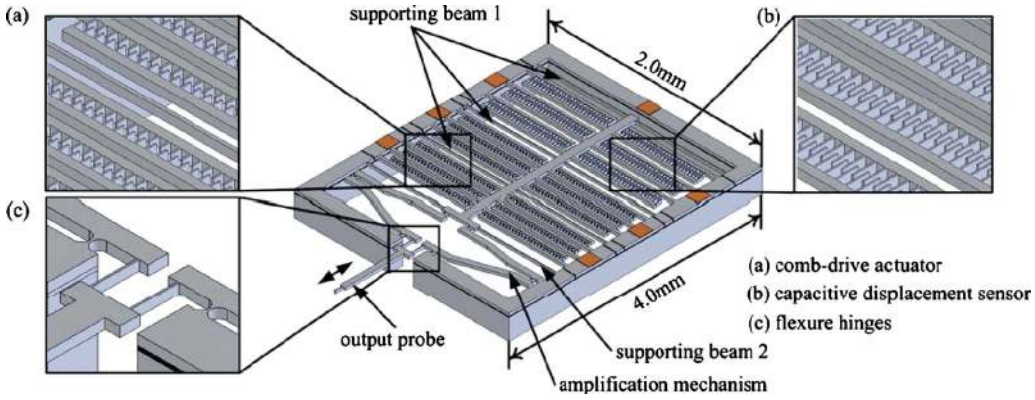

Fig. 16 Solid model of a comb drive nanomanipulator with amplification mechanism and demonstrated motion range of ±2.55 μm with 0.15 nm resolution and force capability of 98 μN [102]

convection, and radiation. For example, consider a control volume for a microcantilever above a substrate, as shown in Fig. 18. Under steady-state conditions, the heating of the element due to the Joule effect balances the heat loss from the element (e.g., due to conduction) [56],

$$Q_x + Q_{\text{Joule}} = Q_{x+dx} + Q_{\text{subs}} \tag{3}$$

In particular, the two conduction terms Q_x and Q_{x+dx} are proportional to the spatial temperature gradient (dT/dx) at the boundaries of the control volume. The heat generated by the Joule effect depends on the element's resistivity and the current density. Heat transfer via conduction to the substrate is impacted by the shape of the element and the thermal resistance between the cantilever and substrate [116].

Equation (3) can be reduced to a second order differential equation and the temperature distribution is solved by applying temperature boundary conditions [56]. The temperature distribution is considered as one dimensional [56], where temperature varies along the length and is uniform across other dimensions. This assumption is valid for Biot number less than 0.1 [117,118] (10^{-5}–10^{-6} for microactuators), which indicates higher heat flow along the length as compared with other directions [71].

With knowledge of the temperature distribution by solving Eq. (3), the linear thermal expansion of the arms can be calculated from the average change in temperature. Next, various methods such as the force method [56] or matrix displacement method [113] can be used to calculate forces, moments, and deflection of the microactuator structure.

It is emphasized that heat lost due to radiation is a mere 1% even at high temperature (~1000°C) [57]. Also, based on Huang and Lee's [56] analysis, heat energy due to resistive heating is 28 times higher than heat loss due to radiation at an operating power of 30 mW. Similar analysis with and without convective and radiation heat transfer depicts minor variation (~10°C) in temperature profile only at high temperatures (~600°C), primarily due to radiation [113]. At the microscale, considering the extremely small characteristic dimensions, the Grashoff [119] and Rayleigh numbers [118] (readers are directed to Ref. [12] for a brief description of microscale heat transfer and significance of the dimensionless numbers), which signify free convective heat transfer, are significantly low ($\sim 10^{-8}$). Therefore, convective heat transfer is not included in most models. Also, microactuators are designed to operate at low power (low temperature) and heat transfer due to radiation can be neglected. Under conditions of a small air gap (~2 μm) between the microactuator and substrate, as shown in Fig. 18, conductive heat transfer is dominant instead of convection (typical conductive heat-transfer coefficient ~15000 $\text{W/m}^2\,\text{K}$ and convective heat-transfer coefficient $=100\ \text{W/m}^2\,\text{K}$ [118]) [57]. Also, conduction takes place through the anchors, which is analytically modeled by temperature boundary conditions.

Analytical models for the various electrostatic designs can be found in the cited references in Sec. 4.1. The simplest electrostatic

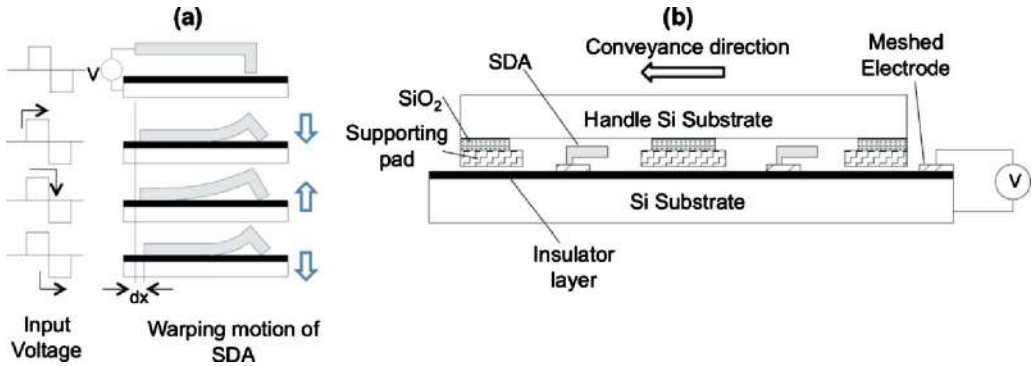

Fig. 17 Schematic diagram of the high force and displacement capable scratch drive actuator (SDA): (*a*) basic configuration showing warping motion of the SDA controlled by amplitude and frequency of input voltage [41]; (*b*) microtranslational table operated by SDA with voltage applied to the SDA by a meshed electrode [112]

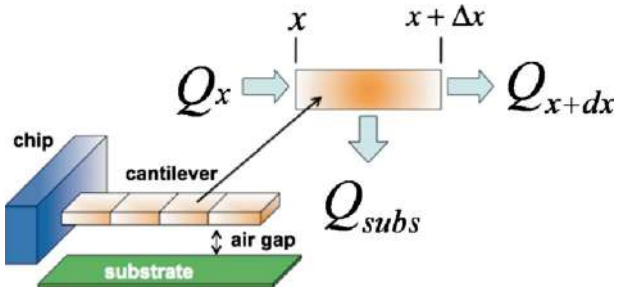

Fig. 18 Schematic diagram showing heat transfer (conduction) from a control volume with internal Joule heating; convection is neglected

actuator is the basic parallel-plate capacitor. The electrostatic attraction force between the two plates is proportional to the gradient of the stored electric energy. The force is given by [120]:

$$F = \frac{CV^2}{2d} \tag{4}$$

where C is the capacitance, d is the separation distance between the two plates, and V is the applied voltage. It is noted that the force drops off considerably with the separation distance d; thus the force generated by electrostatic actuators is most effective over small ranges.

Electrostatic actuators are often designed such that one movable plate is supported by a mechanical spring or flexure with spring constant k_m. In this case, under low frequency or constant applied voltage, the actuator experiences an equilibrium displacement in which the electrostatic force balances the spring force [120].

4.2.2 Challenges. Analytical models for electrothermal microactuators are generally one dimensional and include simplifying assumptions. For example, the empirical relation for conduction shape factor is approximate and sometimes overestimates the cooling and gives lower bound predictions [115,121]. Resistivity is often assumed to vary linearly with temperature [56]. Also, it is difficult to include nonlinear terms such as temperature-dependent properties, thermoelastic deformation, and radiation due to the complexity of obtaining a closed-form solution. Due to these simplifications, research has shown 10% deviation in deflection from experimental data [56,115]. Analysis by Enikov et al. [115] showed 12.5% error in deflection without considering nonlinear thermoelastic deformation. Hickey et al. [118] reported 50% deviation between experimental and transient responses due to nonlinearity in experimental measurement, temperature dependency of properties, and one-dimensional approximation of the analytical model. Thus, microactuators for nanoapplications require improved performance prediction, which may not be available from simple analytical models.

Appropriate modeling and boundary conditions are critical for electrothermal microactuators, especially for the complex heat-transfer mechanisms at the micro- and nanoscales. Thermal boundary condition (TBC) at the anchors can be applied in two different ways [122]: (i) ambient temperature TBC (called *essential boundary condition* (EBC)) with anchors acting as heat sinks when the substrate is *thermally grounded* with large mass at ambient temperature; otherwise the (ii) *natural boundary condition* (NBC) is applied by modeling an insulating medium "restricting heat loss to substrate." The NBC model shows 66.5% higher deflection and is 400% more energy efficient than EBC boundary condition. The heat-transfer mechanism also changes with variation in air gap between the microactuator bottom surface and substrate [117], i.e., convective heat transfer for large air gap ($\sim$450 μm) [122], while conduction dominates at small air gaps ($\sim$2 μm) [118]. Different approaches have been followed for modeling the convective and conductive heat transfer. Krecinic et al. [48] used empirical relations for free convective heat transfer on a horizontal cylinder with an effective diameter calculated from the characteristic (length and cross-sectional area) dimensions. Mankame and Ananthasuresh [122] used an empirical correlation given by Mills [123] for determining the temperature and size dependent convective coefficients. The correlation had to be extrapolated due to lack of published data for Rayleigh numbers for microstructures. However, a recent study by Ozsun et al. [12] speculated on the validity of free convective heat transfer considered in various studies [48,59,64,68,122]. They also investigated and compared macroscale and microscale heat transfers by transient thermal analysis both in fluid (convection) and solid medium (conduction). Free convective heat transfer, which depends on the Rayleigh number, is typically small for microstructures and can be neglected.

Conduction is cited to be the only mode of heat transfer for electrothermal microactuators [12,56,57,119]. For modeling conduction, Geisberger et al. [119] used a three-dimensional finite element (FE) model where conductive air elements were used in the air gap between the actuator and substrate, and hot arm and cold arms. However, this makes the computational domain more complex. An approximate approach to model conductive heat flux as a boundary condition is by substituting an equivalent convective thin film coefficient $\hbar$ calculated based on one-dimensional analysis of the heat conduction from microactuator to substrate [122,124]. An experimental approach for computation of $\hbar$ developed by Oszun et al. [12] is based on determination of the thermal time constant (time required to reach thermal equilibrium $<$ time required to reach maximum deflection). Boundary layer thickness can then be calculated based on the empirical relation with thermal time constant. Computational fluid dynamics based on the boundary layer thickness and characteristic dimension of the microactuator gives the convective thin film coefficient. However, this method relies on accurate measurement of the thermal time constant by high-resolution temperature measurement methods. Despite the advances, consistent, simpler, and effective modeling guidelines are still lacking for electrothermal microactuators.

Very few studies for extracting parametric forms of temperature-dependent material properties for use in FE analysis of electrothermal microactuators have been developed [119]. Also, considering the small dimensions of microactuators, material properties vary significantly from the bulk material [125] and require reliable and accurate testing methods. Material properties such as electrical conductivity, thermal conductivity, Young's modulus, coefficient of thermal expansion, specific heat, resistivity, and convective heat coefficient may vary ($\sim$20–130%) with temperature [122]. Therefore, assuming constant properties shows large variation in performance (deflection versus power) with experimental data [121,124]. Sensitivity studies on a nickel V-beam actuator with variation (0–55000 $\mathrm{W/m^2\,K}$) in temperature dependence heat convection coefficient depicts 1492%, 995%, and $-$24% influence on displacement, temperature, and electrical current, respectively, while a 15–30% variation in thermal expansion coefficient and resistivity show 7–30% variation in displacement, temperature, and electrical current [126]. However, change in Young's modulus and thermal conductivity does not have much impact. For boron-doped single crystal silicon (SCS), temperature dependence of resistivity and thermal conductivity are included in the model as they vary by a factor of 3 in the operating range of temperature [71]. The above facts clearly highlight the significance of using accurate material properties and their variation with temperature for designing high performance and robust electrothermal microactuators.

The key challenges in analytical modeling and analysis of electrostatic microactuators arise from the need to account for the various types of nonlinearities, which may be induced due to spring force, electrostatic force, thermal heating, residual stress and dimensional variation in microfabrication [127]. Under such conditions, design tools for modeling the mechanical spring based

on a linear assumption, small deflection theory, and two-dimensional analysis without including beam rotation can lead to significant design errors [91,107]. Out-of-plane rotation can cause misalignment of the comb fingers leading to pull-in instability. In compliant mechanism, improper design of the suspension system with reduced stiffness can lead to "nondeterministic motion" and end-effector rotation [99]. Also, considering the small dimensions of the structures high stress in flexures and hinges may cause stress stiffening and plastic deformation.

In general, analytical models for the electrostatic microactuators do not include effects of fringing fields, parasitic capacitance due to layout, ground plane levitation effects, and deformation of moving plate, all of which can vary the electrostatic forces by a large magnitude [108]. The fringing field becomes significant when the gap spacing between the electrodes cannot be neglected in comparison to the lateral dimensions and for typical cases the electrostatic forces can increase by 25% [86,128]. In addition, modeling and control in the presence of the various parasitic capacitances and parameter uncertainties are extremely challenging [129]. For actuators driven by multiple voltage sources, dynamic pull-in instability may occur due to the instantaneous application of voltage [130]. Casimir force and van der Waals force are seen to be dominant in the small dimensions (100 nm range) and affect the pull-in voltage [131].

Performance analysis due to variation in profile during microfabrication seem to have significant effect on the electrostatic force, displacement, and damping of the electrostatic microactuator [9,10]. For instance, relative displacement was 1.58 times the design displacement due to tapered etching profile of the flexures and comb-electrodes [10]. Therefore, a closer performance prediction can be obtained by three-dimensional mapping of the actuator. Although, simple analytical models can be developed for tapering profiles but complex three-dimensional shapes by FE analysis will lead to a predictable design.

4.3 Sensing and Experimental Methods for Actuator Performance Characterization. Accurate and reliable methods give feedback for optimized design and fabrication of the microactuators. A brief overview of the different methods used for measurement of motion (displacement), force, temperature, and dynamic characteristics is given in this section.

Motion measurement with nanometer accuracy and fast response speed is required for microactuator performance evaluation at the nanoscale. Computer vision methods using charged coupled device (CCD) with robust motion estimation algorithms have demonstrated resolution better than 10 nm [132]. Motion resolution less than 3 nm is reported by Liu et al. [102] using a high magnification optical lens with a commercial digital camera. Laser Doppler systems [133] are advantageous as they can measure arbitrary motion (resonant frequency and transient velocity) compared with image processing methods, which detect periodic repeatable motion. However, the discrepancy at higher amplitudes needs to be improved. Interferometery-based techniques that operate on the change in fringe pattern have been used for measuring out-of-plane deflections [70]. For in situ position measurements inside high-resolution SEM, micromanipulators with 1.55 nm resolution and nanopositioning stage with a resolution of approximately 0.25 nm were used [43,67]. A list of commercially available manipulators with details on motion range, degree-of-freedom, and resolution can be found in Ref. [74]. Some novel methods such as epifluorescence microscopy with positional accuracy in the range of 4 nm have potential use in the future [134].

Measurement of forces ranging from piconewton to millinewton can be done by methods such as cantilever-based sensors, acupuncture needles, AFM probes, and MEMS-based capacitive force sensors that are summarized in Refs. [135–137]. The sensitivity of cantilever-based method depends on the beam stiffness and its accurate calibration. The AFM probes used for measurement of stiffness have demonstrated resolution down to 0.1 pN/nm [138]. MEMS-based capacitive sensors are advantageous with their multiaxis force measurement capability, high sensitivity, and wide range from millinewton to piconewton [136].

Submicron scale spatial resolution temperature measurement methods are required for mapping the temperature distribution in electrothermal actuators. Sweep and sampling methods that relate the temperature-dependent resistance change with voltage for measurement of steady-state temperature and response are inadequate [48]. Thermography-based methods provide spatial resolution ~ 1.5 μm; however, bias errors are present due to dependence on emissivity. A near infrared wavelength (450 nm) detector coupled with a CCD camera with less dependence on emissivity and higher resolution has been studied by Teyssieux et al. [139]. Raman microscopy has been used for temperature measurement and imaging within a spatial resolution of 0.5 μm [140]. However, Raman microscopy needs extended exposure and is suitable for steady-state conditions with demonstrations up to approximately 100 μs temporal resolution [141].

The dynamic response of an actuator reveals important information such as resonance frequencies, operating bandwidth, and potential cross-coupling effects. During the initial design phase, finite element analysis tools can be used to predict in-plane and out-of-plane mode shapes and resonant frequencies. Experimental characterization is often performed by exciting the actuator and measuring its response to create frequency response functions. Commercially available dynamic signal analyzers in conjunction with optical displacement sensors are specifically designed to acquire frequency response functions over a wide range of operating conditions. Scanning laser vibrometers are now capable of measuring structural mode shapes in 3D for MEMS devices such as microcantilevers [142].

5 Fabrication Techniques

There is a wide range of MEMS-based microfabrication techniques and materials that are used to create the microactuators. Integrated circuit (IC) and MEMS microfabrication techniques are at a mature level and are well documented. For in-depth reviews and details of microfabrication techniques and materials, Refs. [143–145] are recommended. Here, we briefly discuss several general microfabrication processes and associated issues that must be considered for the microactuator fabrication.

5.1 Microfabrication. Selection of the microactuator fabrication process depends upon the specific application, material, tolerance, and size of features (e.g., thickness and aspect ratio). Bulk micromachining is preferred for structures with thickness greater than 10 μm and surface micromachining for thinner structures [1]. Surface micromachining [144] is a method of depositing sacrificial layers and structural layers combined with selective etching and patterning to fabricate complex microstructures ($1-10$ μm) thick [1]. Significant advantages of this method are thinner structures with higher tolerance and smaller footprint. However, mechanical stress may be developed in the various deposited layers [103]. Bulk micromachining is a process combining layer deposition, etching, and patterning of a single crystal, typically a silicon substrate, to machine out the geometry of the microactuator. The two most common methods employ silicon-on-insulator (SOI) based and single crystal reactive etching and metallization (SCREAM) processes.

SCREAM utilizes reactive ion etching (RIE) to fabricate suspended structures that are released from a silicon wafer. The key steps involve transfer of a pattern to a silicon oxide layer on silicon followed by RIE to a specified depth to form the device structure in silicon. A conformal passivating material layer is deposited over the device structure. A small gap at the base of the device structure is made by an additional RIE step followed by a final etch to release the structure. SCREAM typically uses a single mask process for fabrication of metal microactuators. A silicon nitride layer can be used as an etch mask, a sacrificial layer for

releasing microstructures, and as an electrically insulating layer for metal electrodes. A drawback of the SCREAM process is that it can create residual stresses in the device structure due to the conformal deposition step that can cause unwanted buckling or fracture of the device structure. The residual stress problem is an even more important consideration for submicron and high-aspect ratio features.

SOI processes are now most commonly used in MEMS fabrication, especially for fabrication of microactuators [2,43]. SOI wafers consist of a handle layer, silicon dioxide layer (typically 1 μm), and a device layer (typically chosen to be the thickness of a microactuator). SOI processes involve patterning of the silicon device and handle layers into the desired device geometry followed by a selective etch through the handle layer and sacrificial oxide to release the device structure (e.g., typical process for fabrication of cantilever actuators). One significant problem in the use of SOI substrates is the variation in silicon layer thickness and uniformity; as a result, material properties and device performance can vary significantly. There has been considerable progress made in reducing variation with the introduction of the Smart-Cut® process [146]. Uniformity better than ± 3 nm has been achieved; however, a key challenge remains to achieve <1 nm thickness uniformity.

Micromolding processes, including (i) Hexsil, (ii) HARPSS, and (iii) LIGA lithography, electroplating (galvanoformung), and molding (abformtechnik) are used for fabricating high-aspect ratio microstructures [1]. The Hexsil process begins with RIE trench etching of silicon. This is followed by deposition of oxide and structural (polysilicon) layers. Then, the sacrificial layer is removed by etching and the polysilicon structural layer can be released. The LIGA process begins with deposition of a sacrificial layer on a substrate with a seed layer (metal plating). A sheet of polymethyl methacrylate (PMMA) is coated on the substrate, which is then exposed selectively to X-Rays through a suitable mask that absorbs X-Rays. This process transfers the pattern onto the PMMA that now acts as a mold. Structural material (metal) can then be deposited in the mold. Dissolving the PMMA crystal in a suitable solvent releases the microstructure. One drawback of LIGA is the need for high-energy X-Ray sources, such as synchrotrons or linear accelerators that are of limited availability and high cost. Standard photolithography of SU-8 is a much less expensive alternative and has similar capabilities as LIGA.

5.2 Nanofabrication. As microactuator features scale further down in size and future development of nanoactuators progress, nanofabrication approaches must be considered. Patterning methods include electron beam, focused ion beam, extreme UV, soft, and nanoimprint lithographies [147]. Soft lithography, also known as microcontact printing, is an extremely versatile approach for fabrication of chemical and biological applications where patterning and modification of polymer surfaces predominate. Nanoimprint lithography has a minimum feature resolution less than 10 nm while the other methods approach 20 nm. Recently, nanoimprint lithography has demonstrated wafer scale patterning of sub-40 nm and high-aspect ratio ($>50:1$) silicon pillars [148]. Scanning probe lithography approaches, including scanning tunneling microscopy [149], atomic force microscopy [150], and dip pen [21], have potentially the highest resolution (<1 nm) using atomically sharp probe tips; however, these processes are relatively slow and low throughput. Progress to increase throughput is being made. Recently, polymer pen lithography has demonstrated large area printing and patterning with relatively high throughput by utilizing 11×10^6 tips in the form of a soft stamp [151].

6 Future Directions

Further research is required in various aspects of new design tools, materials and fabrication processes, force modeling and simulation, control and automation methods, parallelism, and scalability for large-scale operations.

6.1 Advanced Design Methodologies. The small design space available for microactuators imposes a major challenge to obtain an optimized design satisfying the strength, stiffness, dynamic response, and deflection required for various nanoscale applications. A minor change in the design and modeling parameters can result in a drastic change in the operating characteristics. Under such conditions, advanced design methods such as FE with optimization techniques [152], topology optimization with perturbation based design [153], and genetic algorithms [154] can produce optimized output such as force, flexibility, and displacement by solving the multiobjective and multiconstraint function. Manufacturing tolerant design [155] and reliability-based optimization methods [156] that include fabrication uncertainties such as profile variation due to irregular etching can ensure robust performance. Also, advanced approaches such as meshless methods show promising potential to address the numerical errors and degenerate solutions for the highly complex, nonlinear, multiphysics microactuator problem [157]. Therefore, further advancement of design tools with integrated optimization techniques will be required well into the future.

6.2 Physics-Based Modeling. Design guidelines for heat-transfer mechanisms, boundary conditions, and conduction shape factor for electrothermal actuators have not been well established. Also, as actuator size scales down to the nanoscale level, the Thomson effect becomes significant as compared with conduction and radiation [11]. This effect must be accounted for in analytical and finite element models.

Physics based continuum mechanics and molecular dynamics models need to be developed to accurately predict the nanoscale forces and the actuator tip-sample interaction. Simulation of the forces under different operating modes such as pushing, pulling, bending, orienting, and detaching that take into account the effect of material properties, surface topology, and environmental effects is required for accurate performance prediction. Such simulations will promote development of alternative nanomanipulation approaches including noncontact handling systems such as electrostatic and magnetic levitation techniques [158].

6.3 Material Properties and Fabrication. The scope of improving the performance of microactuators will depend significantly upon the utilization of various material combinations and potentially the unique properties of new nanostructured materials. However, material properties at the nanoscale differ from the bulk properties. A material databank of material properties at nanoscale is not available. Further, there has been limited investigation in extraction of temperature-dependent material models required for accurate prediction of the actuator performance. In addition, future developments have to include new measurement standards and procedures for consistent and reliable data [159]. Fabrication methods need improvement in various aspects including high-yield batch fabrication, high-aspect ratio feature uniformity, minimum process deviations, minimum residual stress, high strength, and fatigue properties.

6.4 Control, Sensing, Automation, and Scalability. Large scale manufacturing with high throughput requires an array of microactuators. This entails development of in situ performance measurement methods and inspection techniques for online monitoring. Additionally, advanced control schemes (for multi-input, multi-output systems) are needed for precision operation. Automated tool changing systems are also required for handling the multiple microactuators for different operations and replacement of damaged microactuators.

Integrated contact and force sensing methods have been demonstrated, but are mostly limited to piezoresistive and capacitive based sensing. Higher resolution, sensitivity, and bandwidth are required. In summary, challenges exist in highly parallel actuation and sensing capabilities in terms of assembly, electrical connection, programming, and control.

7 Conclusion

Nanoscale manufacturing is an emerging field that requires tools and processes capable of precisely positioning and manipulating nanoscale components and materials. This paper reviewed the state-of-the-art in microactuators and related issues in their design, fabrication, and application for nanoscale manufacturing. The basic design considerations for operation of the microactuators at the nanoscale were discussed. Emerging challenges in modeling, analysis, and performance characterization based on a review of the literature were elaborated. Current and emerging applications of microactuators for nanoscale manipulation and nanobiotechnology were reported. Future directions have been identified to address limitations of the emerging tools.

Acknowledgment

This work is supported by the National Science Foundation under Grant CMMI No. 0910570. The authors are grateful to the authors and publishers of the research papers included in this review, especially for granting permission for using their copyright images in this paper. The authors would also like to thank the University of Florida Machine Tool Research Center members for their insightful discussions and feedback.

References

[1] Fedder, G. K., 2003, "MEMS Fabrication," Proceedings of the 33rd International Test Conference, pp. 691–698.
[2] Sardan, O., Eichhorn, V., Petersen, D. H., Fatikow, S., Sigmund, O., and Boggild, P., 2008, "Rapid Prototyping of Nanotube-Based Devices Using Topology-Optimized Microgrippers," Nanotechnology, **19**(49), p. 495503.
[3] Kimberly, T., Matthew, E., Aaron, G., George, S., and Phil, F., 2004, "FIB Prepared TEM Sample Lift-Out Using MEMS Grippers," Microsc. Microanal., **10**, (S02), pp. 1144–1145.
[4] Chronis, N., and Lee, L. P., 2005, "Electrothermally Activated SU-8 Microgripper for Single Cell Manipulation in Solution," J. Microelectromech. Syst., **14**(4), pp. 857–863.
[5] Kim, K., Liu, X., Zhang, Y., and Sun, Y., 2008, "Nanonewton Force-Controlled Manipulation of Biological Cells Using a Monolithic MEMS Microgripper With Two-Axis Force Feedback," J. Micromech. Microeng., **18**(5), p. 055013.
[6] Requicha, A. A. G., 2003, "Nanorobots, NEMS, and Nanoassembly," Proc. IEEE, **9**, pp. 1922–1933.
[7] Devasia, S., Eleftheriou, E., and Moheimani, S. O. R., 2007, "A Survey of Control Issues in Nanopositioning," IEEE Trans. Control Syst. Technol., **15**(5), pp. 802–823.
[8] Haliyo, D. S., Regnier, S., and Guinot, J.-C., 2003, "[mü]MAD, the Adhesion Based Dynamic Micro-Manipulator," Eur. J. Mech. A/Solids, **22**(6), pp. 903–916.
[9] Li, J., Liu, A. Q., and Zhang, Q. X., 2006, "Tolerance Analysis for Comb-Drive Actuator Using DRIE Fabrication," Sens. Actuators, A, **125**(2), pp. 494–503.
[10] Chen, B., and Miao, J., 2007, "Influence of Deep RIE Tolerances on Comb-Drive Actuator Performance," J. Phys. D: Appl. Phys., **40**(4), pp. 970–976.
[11] Jungen, A., Pfenninger, M., Tonteling, M., Stampfer, C., and Hierold, C., 2006, "Electrothermal Effects at the Microscale and Their Consequences on System Design," J. Micromech. Microeng., **16**(8), pp. 1633–1638.
[12] Ozsun, O., Alaca, B. E., Yalcinkaya, A. D., Yilmaz, M., Zervas, M., and Leblebici, Y., 2009, "On Heat Transfer at Microscale With Implications for Microactuator Design," J. Micromech. Microeng., **19**(4), p. 045020.
[13] Kiuchi, M., Matsui, S., and Isono, Y., 2007, "Mechanical Characteristics of FIB Deposited Carbon Nanowires Using an Electrostatic Actuated Nano Tensile Testing Device," J. Microelectromech. Syst., **16**(2), pp. 191–201.
[14] Zhu, Y., Corigliano, A., and Espinosa, H. D., 2006, "A Thermal Actuator for Nanoscale In Situ Microscopy Testing: Design and Characterization," J. Micromech. Microeng., **16**(2), pp. 242–253.
[15] Haque, M. A., 2005, "In Situ Tensile Testing of Nanoscale Freestanding Thin Films Inside a Transmission Electron Microscope," J. Mater. Res., **20**(7), pp. 1769–1777.
[16] Haque, M. A., and Saif, M. T. A., 2002, "Application of MEMS Force Sensors for In Situ Mechanical Characterization of Nano-Scale Thin films in SEM and TEM," Sens. Actuators, A, **97–98**, pp. 239–245.
[17] Wilson, N. R., and Macpherson, J. V., 2009, "Carbon Nanotube Tips for Atomic Force Microscopy," Nat. Nanotechnol., **4**(8), pp. 483–491.
[18] Piner, R. D., Zhu, J., Xu, F., Hong, S., and Mirkin, C. A., 1999, "Dip-Pen Nanolithography," Science, **283**, pp. 661–663.
[19] Bullen, D., Wang, X., Zou, J., Chung, S., Mirkin, C. A., and Liu, C., 2004, "Design, Fabrication, and Characterization of Thermally Actuated Probe Arrays for Dip Pen Nanolithography," J. Microelectromech. Syst., **13**(4), pp. 594–602.
[20] Bullen, D., and Liu, C., 2006, "Electrostatically Actuated Dip Pen Nanolithography Probe Arrays," Sens. Actuators, A, **125**(2), pp. 504–511.
[21] Salaita, K., Wang, Y., and Mirkin, C. A., 2007, "Applications of Dip-Pen Nanolithography," Nat. Nanotechnol., **2**(3), pp. 145–155.
[22] Bullen, D., Chung, S. W., Wang, X., Zou, J., and Mirkin, C. A., 2004, "Parallel Dip-Pen Nanolithography With Arrays of Individually Addressable Cantilevers," Appl. Phys. Lett., **84**(5), pp. 789–791.
[23] Li, S., Liu, C., and Wang, X., 2006, "Multifunctional Probe Array and Local Vapor Inking Chip for Scanning Probe Nanolithography," Sixth IEEE Conference on Nanotechnology, IEEE-NANO 2006, Vol. 2, pp. 551–554.
[24] Wang, X., Bullen, D., Zou, J., Liu, C., and Mirkin, C. A., 2004, "Thermally Actuated Probe Array for Parallel Dip-Pen Nanolithography," J. Vac. Sci. Technol. B, **22**, pp. 2563–2567.
[25] Salaita, K., Wang, J., Fragala, J., Vega, R. A., Liu, A. Q., and Mirkin, C. A., 2006, "Massively Parallel Dip-Pen Nanolithography With 55 000-Pen Two-Dimensional Arrays," Angew. Chem., Int. Ed., **45**(43), pp. 7220–7223.
[26] Dario, P., Carrozza, M. C., Benvenuto, A., and Menciassi, A., 2000, "Micro-Systems in Biomedical Applications," J. Micromech. Microeng., **10**(2), pp. 235–244.
[27] Du, S. E., Cui, H., and Zhu, Z., 2006, "Review of Nanomanipulators for Nanomanufacturing," International Journal of Nanomanufacturing, **1**(1), pp. 83–104.
[28] Shibata, T., Yamanaka, S., Kato, N., Kawashima, T., Nomura, M., Mineta, T., and Makino, E., 2009, "Fabrication of Micromanipulator Array for Cell Patterning," Microelectron. Eng., **86**(4–6), pp. 1439–1442.
[29] Alonso, J. L., and Goldmann, W. H., 2003, "Feeling the Forces: Atomic Force Microscopy in Cell Biology," Life Sci., **72**(23), pp. 2553–2560.
[30] Fatikow, S., and Eichhorn, V., 2008, "Nanohandling Automation: Trends and Current Developments," Proc. Inst. Mech. Eng., Part C: J. Mech. Eng. Sci., **222**(7), pp. 1353–1369.
[31] De Vries, A. H. B., Krenn, B. E., Van Driel, R., and Kanger, J. S., 2005, "Micro Magnetic Tweezers for Nanomanipulation Inside Live Cells," Biophys. J., **88**(3), pp. 2137–2144.
[32] Inoue, K., Tanikawa, T., and Arai, T., 2008, "Micro-Manipulation System With a Two-Fingered Micro-Hand and Its Potential Application in Bioscience," J. Biotechnol., **133**(2), pp. 219–224.
[33] Bell, D. J., Lu, T. J., Fleck, N. A., and Spearing, S. M., 2005, "MEMS Actuators and Sensors: Observations on Their Performance and Selection for Purpose," J. Micromech. Microeng., **15**(7), pp. S153–S164.
[34] Hubbard, N. B., Culpepper, M. L., and Howell, L. L., 2006, "Actuators for Micropositioners and Nanopositioners," Appl. Mech. Rev., **59**(6), pp. 324–334.
[35] Leang, K.K., Zou, Q., and Devasia, S., 2009, "Feedforward Control of Piezoactuators in Atomic Force Microscope Systems: Inversion-Based Compensation for Dynamics and Hysteresis," IEEE Trans. Control Syst. Technol., **19**(1), pp. 70–82.
[36] Muralt, P., 2008, "Recent Progress in Materials Issues for Piezoelectric MEMS," J. Am. Ceram. Soc., **91**(5), pp. 1385–1396.
[37] Jeon, C. S., Park, J. S., Lee, S. Y., and Moon, C. W., 2007, "Fabrication and Characteristics of Out-of-Plane Piezoelectric Microgrippers Using MEMS Processes," Thin Solid Films, **515**(12), pp. 4901–4904.
[38] Bechtold, T., Rudnyi, E., and Korvink, J., 2005, "Dynamic Electro-Thermal Simulation of Microsystems—A Review," J. Micromech. Microeng., **15**(11), pp. R17–R31.
[39] Comtois, J. H., and Bright, V. M., 1997, "Applications for Surface-Micromachined Polysilicon Thermal Actuators and Arrays," Sens. Actuators, A, **58**(1), pp. 19–25.
[40] Greitmann, G., and Buser, R. A., 1996, "Tactile Microgripper for Automated Handling of Microparts," Sens. Actuators, A, **53**(1–3), pp. 410–415.
[41] Geisberger, A., and Sarkar, N., 2006, *MEMS/NEMS: Techniques in Microelectrothermal Actuator and Their Applications*, Springer, New York.
[42] Imamura, T., Katayama, M., Ikegawa, Y., Ohwe, T., Koishi, R., and Koshikawa, T., 1998, "MEMS-Based Integrated Head/Actuator/Slider for Hard Disk Drives," IEEE/ASME Trans. Mechatron., **3**(3), pp. 166–174.
[43] Andersen, K. N., Petersen, D. H., Carlson, K., Molhave, K., Sardan, O., Horsewell, A., Eichhorn, V., Fatikow, S., and Boggild, P., 2009, "Multimodal Electrothermal Silicon Microgrippers for Nanotube Manipulation," IEEE Trans. Nanotechnol., **8**(1), pp. 76–85.
[44] Chang, J., Min, B., Kim, J., and Lin, L., 2009, "Bimorph Nano Actuators Synthesized by Focused Ion Beam Chemical Vapor Deposition," Microelectron. Eng., **86**(11), pp. 2364–2368.
[45] Mølhave, K., Wich, T., Kortschack, A., and Bøggild, P., 2006, "Pick-and-Place Nanomanipulation Using Microfabricated Grippers," Nanotechnology, **17**(10), pp. 2434–2441.
[46] Petrina, A., and Petrin, A., 2008, "On the Question of Information Processing in Nanomanipulation Tasks," Automatic Documentation and Mathematical Linguistics, **42**(2), pp. 136–142.
[47] Mølhave, K., and Hansen, O., 2005, "Electro-Thermally Actuated Microgrippers With Integrated Force-Feedback," J. Micromech. Microeng., **15**(6), pp. 1265–1270.
[48] Krecinic, F., Duc, T. C., Lau, G. K., and Sarro, P. M., 2008, "Finite Element Modelling and Experimental Characterization of an Electro-Thermally Actuated Silicon-Polymer Microgripper," J. Micromech. Microeng., **18**(6), p. 064007.
[49] Prasanna, S., and Spearing, S. M., 2007, "Material Selection and Design of Microelectrothermal Bimaterial Actuators," J. Microelectromech. Syst., **16**(2), pp. 248–259.
[50] Srikar, V. T., and Spearing, S. M., 2003, "Materials Selection for Microfabri-

cated Electrostatic Actuators," Sens. Actuators, A, **102**(3), pp. 279–285.
[51] Zhou, Q., Chang, B., and Koivo, H. N., 2004, "Ambient Environmental Effects in Micro/Nano Handling," Fourth International Workshop on Microfactories-IWMF, Shanghai, China, pp. 146–151.
[52] Chen, S.-C., and Culpepper, M. L., 2006, "Design of a Six-Axis Micro-Scale Nanopositioner-[mu]HexFlex," Precis. Eng., **30**(3), pp. 314–324.
[53] Hikihara, T., 2009, *Applications of Nonlinear Dynamics: Dynamics in Manipulation and Actuation of Nano-Particles*, Springer, Berlin, Heidelberg.
[54] Lee, C. C., and Hsu, W., 2003, "Optimization of an Electro-Thermally and Laterally Driven Microactuator," Microsyst. Technol., **9**(5), pp. 331–334.
[55] Guckel, H., Klein, J., Christenson, T., Skrobis, K., Laudon, M., and Lovell, E. G., 1992, "Thermo-Magnetic Metal Flexure Actuators," Fifth Technical Digest, IEEE Solid-State Sensor and Actuator Workshop, pp. 73–75.
[56] Huang, Q., and Lee, N. K. S., 1999, "Analysis and Design of Polysilicon Thermal Fexure Actuator," J. Micromech. Microeng., **9**, pp. 64–70.
[57] Hickey, R., Kujath, M., and Hubbard, T., 2002, "Heat Transfer Analysis and Optimization of Two-Beam Microelectromechanical Thermal Actuators," J. Vac. Sci. Technol. A, **20**(3), pp. 971–974.
[58] Kolesar, E. S., Allen, P. B., Howard, J. T., Wilken, J. M., and Boydston, N., 1999, "Thermally-Actuated Cantilever Beam for Schieving Large In-Plane Mechanical Deflections," Thin Solid Films, **355–356**, pp. 295–302.
[59] Chen, R. S., Kung, C., and Lee, G.-B., 2002, "Analysis of the Optimal Dimension on the Electrothermal Microactuator," J. Micromech. Microeng., **12**(3), pp. 291–296.
[60] Lee, J.-S., Park, D. S.-W., Nallani, A. K., Lee, G.-S., and Lee, J.-B., 2005, "Sub-Micron Metallic Electrothermal Actuators," J. Micromech. Microeng., **15**(2), pp. 322–327.
[61] Kolesar, E. S., Ko, S. Y., Howard, J. T., Allen, P. B., Wilken, J. M., Boydston, N. C., Ruff, M. D., and Wilks, R. J., 2000, "In-Plane Tip Deflection and Force Achieved With Asymmetrical Polysilicon Electrothermal Microactuators," Thin Solid Films, **377–378**, pp. 719–726.
[62] Moulton, T., and Ananthasuresh, G., 2001, "Micromechanical Devices With Embedded Electro-Thermal Compliant Actuation," Sens. Actuators, A, **90**(1–2), pp. 38–48.
[63] Yan, D., Khajepour, A., and Mansour, R., 2003, "Modeling of Two-Hot-Arm Horizontal Thermal Actuator," J. Micromech. Microeng., **13**(2), pp. 312–322.
[64] Li, L., and Uttamchandani, D., 2004, "Modified Asymmetric Micro-Electrothermal Actuator: Analysis and Experimentation," J. Micromech. Microeng., **14**(12), pp. 1734–1741.
[65] Henneken, V. A., Tichem, M., and Sarro, P. M., 2008, "Improved Thermal U-Beam Actuators for Micro-Assembly," Sens. Actuators, A, **142**(1), pp. 298–305.
[66] Tsai, L.-N., Shen, G.-R., Cheng, Y.-T., and Hsu, W., 2006, "Performance Improvement of an Electrothermal Microactuator Fabricated Using Ni-Diamond Nanocomposite," J. Microelectromech. Syst., **15**(1), pp. 149–158.
[67] Carlson, K., Andersen, K. N., Eichhorn, V., Petersen, D. H., Molhave, K., Bu, I. Y. Y., Teo, K. B. K., Milne, W. I., Fatikow, S., and Boggild, P., 2007, "A Carbon Nanofibre Scanning Probe Assembled Using an Electrothermal Microgripper," Nanotechnology, **18**(34), p. 345501.
[68] Atre, A., 2006, "Analysis of Out-of-Plane Thermal Microactuators," J. Micromech. Microeng., **16**(2), pp. 205–213.
[69] Yan, D., Khajepour, A., and Mansour, R., 2004, "Design and Modeling of a MEMS Bidirectional Vertical Thermal Actuator," J. Micromech. Microeng., **14**(7), pp. 841–850.
[70] Elbuken, C., Topaloglu, N., Nieva, P., Yavuz, M., and Huissoon, J., 2009, "Modeling and Analysis of a 2-DOF Bidirectional Electro-Thermal Microactuator," Microsyst. Technol., **15**(5), pp. 713–722.
[71] Chen, S. C., and Culpepper, M. L., 2006, "Design of Contoured Microscale Thermomechanical Actuators," J. Microelectromech. Syst., **15**(5), pp. 1226–1234.
[72] Dan, Z., Guifu, D., Lida, Z., and Jifeng, C., 2008, "An Out-of-Plane Electro-Thermal Polymer Actuator," Proceedings of the Third IEEE International Conference on Nano/Micro Engineered and Molecular Systems, Sanya, China, pp. 647–650.
[73] Popa, D. O., Kang, B. H., Wen, J. T., Stephanou, H. E., Skidmore, G., and Geisberger, A., 2003, "Dynamic Modeling and Input Shaping of Thermal Bimorph MEMS Actuators," Proceedings of the ICRA'03 IEEE International Conference on Robotics and Automation, Taipei, Taiwan, Vol. 1, pp. 1470–1475.
[74] Ouyang, P., Tjiptoprodjo, R., Zhang, W., and Yang, G., 2008, "Micro-Motion Devices Technology: The State of Arts Review," Int. J. Adv. Manuf. Technol., **38**(5–6), pp. 463–478.
[75] Ananthasuresh, G. K., and Howell, L. L., 2005, "Mechanical Design of Compliant Microsystems—A Perspective and Prospects," ASME J. Mech. Des., **127**(4), pp. 736–738.
[76] Tsai, Y.-C., Lei, S. H., and Sudin, H., 2005, "Design and Analysis of Planar Compliant Microgripper Based on Kinematic Approach," J. Micromech. Microeng., **15**(1), pp. 143–156.
[77] Jonsmann, J., Sigmund, O., and Bouwstra, S., 1999, "Compliant Electro-thermal Microactuators," 12th IEEE International Conference on Micro Electro Mechanical Systems, pp. 588–593.
[78] Sigmund, O., 2001, "Design of Multiphysics Actuators Using Topology Optimization—Part I: One-Material Structures," Comput. Methods Appl. Mech. Eng., **190**(49–50), pp. 6577–6604.
[79] Sardan, O., Petersen, D. H., Mølhave, K., Sigmund, O., and Bøggild, P., 2008, "Topology Optimized Electrothermal Polysilicon Microgrippers," Microelectron. Eng., **85**(5–6), pp. 1096–1099.
[80] Rubio, W. M., Silva, E. C. N., Bordatchev, E. V., and Zeman, M. J. F., 2008, "Topology Optimized Design, Microfabrication and Characterization of Electro-Thermally Driven Microgripper," J. Intell. Mater. Syst. Struct., **20**(6), pp. 669–681.
[81] Sardan, O., Petersen, D. H., Sigmund, O., and Boggild, P., 2008, "Simulation of Topology Optimized Electrothermal Microgrippers," COMSOL Conference, Hannover, Germany pp. 1–20.
[82] Nguyen, N.-T., Ho, S.-S., and Low, C. L.-N., 2004, "A Polymeric Microgripper With Integrated Thermal Actuators," J. Micromech. Microeng., **14**(7), pp. 969–974.
[83] Solano, B., and Wood, D., 2007, "Design and Testing of a Polymeric Microgripper for Cell Manipulation," Microelectron. Eng., **84**(5–8), pp. 1219–1222.
[84] Duc, T. C., Lau, G.-K., and Sarro, P. M., 2008, "Polymeric Thermal Microactuator With Embedded Silicon Skeleton: Part II—Fabrication, Characterization, and Application for 2-DOF Microgripper," J. Microelectromech. Syst., **17**(4), pp. 823–831.
[85] Lau, E. K., Goosen, J. F. L., Van Keulen, F., Duc, T. C., and Sarro, P. M., 2008, "Polymeric Thermal Microactuator With Embedded Silicon Skeleton: Part I—Design and Analysis," J. Microelectromech. Syst., **17**(4), pp. 809–822.
[86] Elata, D., and Leus, V., 2005, "How Slender Can Comb-Drive Fingers Be?," J. Micromech. Microeng., **15**(5), pp. 1055–1059.
[87] Zhou, G., and Dowd, P., 2003, "Tilted Folded-Beam Suspension for Extending the Stable Travel Range of Comb-Drive Actuators," J. Micromech. Microeng., **13**(2), pp. 178–183.
[88] Hirano, T., Furuhata, T., Gabriel, K. J., and Fujita, H., 1992, "Design, Fabrication, and Operation of Submicron Gap Comb-Drive Microactuators," J. Microelectromech. Syst., **1**(1), pp. 52–59.
[89] Hou, M. T.-K., Huang, G. K.-W., Huang, J.-Y., Liao, K.-M., Chen, R., and Yeh, J.-L. A., 2006, "Extending Displacements of Comb Drive Actuators by Adding Secondary Comb Electrodes," J. Micromech. Microeng., **16**(4), pp. 684–691.
[90] Chen, C., and Lee, C., 2004, "Design and Modeling for Comb Drive Actuator With Enlarged Static Displacement," Sens. Actuators, A, **115**(2–3), pp. 530–539.
[91] Legtenberg, R., Groeneveld, A. W., and Elwenspoek, M., 1996, "Comb-Drive Actuators for Large Displacements," J. Micromech. Microeng., **6**(3), pp. 320–329.
[92] Dai, W., Lian, K., and Wang, W., 2007, "Design and Fabrication of a SU-8 Based Electrostatic Microactuator," Microsyst. Technol., **13**(3–4), pp. 271–277.
[93] Grade, J. D., Jerman, H., and Kenny, T. W., 2003, "Design of Large Deflection Electrostatic Actuators," J. Microelectromech. Syst., **12**(3), pp. 335–343.
[94] Ye, W., and Mukherjee, S., 1999, "Optimal Shape Design of Three-Dimensional MEMS With Applications to Electrostatic Comb Drives," Int. J. Numer. Methods Eng., **45**(2), pp. 175–194.
[95] Sun, L., Wang, J., Rong, W., Li, X., and Bao, H., 2008, "A Silicon Integrated Micro Nano-Positioning XY-Stage for Nano-Manipulation," J. Micromech. Microeng., **18**(12), p. 125004.
[96] Chiou, J.-C., Lin, Y.-J., and Kuo, C.-F., 2008, "Extending the Traveling Range With a Cascade Electrostatic Comb-Drive Actuator," J. Micromech. Microeng., **18**(1), p. 015018.
[97] Liu, X., Kim, K., and Sun, Y., 2007, "A MEMS Stage for 3-Axis Nanopositioning," J. Micromech. Microeng., **17**(9), pp. 1796–1802.
[98] Gu, L., Li, X., Bao, H., Liu, B., Wang, Y., Liu, M., Yang, Z., and Cheng, B., 2006, "Single-Wafer-Processed Nano-Positioning XY-stages With Trench-Sidewall Micromachining Technology," J. Micromech. Microeng., **16**(7), pp. 1349–1357.
[99] Dong, J., Mukhopadhyay, D., and Ferreira, P. M., 2007, "Design, Fabrication and Testing of a Silicon-on-Insulator (SOI) MEMS Parallel Kinematics XY Stage," J. Micromech. Microeng., **17**(6), pp. 1154–1161.
[100] Mukhopadhyay, D., Dong, J., Pengwang, E., and Ferreira, P., 2008, "A SOI-MEMS-Based 3-DOF Planar Parallel-Kinematics Nanopositioning Stage," Sens. Actuators, A, **147**(1), pp. 340–351.
[101] Yao, Q., Dong, J., and Ferreira, P. M., 2008, "A Novel Parallel-Kinematics Mechanisms for Integrated, Multi-Axis Nanopositioning: Part 1. Kinematics and Design for Fabrication," Precis. Eng., **32**(1), pp. 7–19.
[102] Liu, X., Tong, J., and Sun, Y., 2007, "A Millimeter-Sized Nanomanipulator With Sub-Nanometer Positioning Resolution and Large Force Output," Smart Mater. Struct., **16**(5), pp. 1742–1750.
[103] Volland, B. E., Heerlein, H., and Rangelow, I. W., 2002, "Electrostatically Driven Microgripper," Microelectron. Eng., **61–62**, pp. 1015–1023.
[104] Chang, H.-C., Tsai, J. M.-L., Tsai, H.-C., and Fang, W., 2006, "Design, Fabrication, and Testing of a 3-DOF HARM Micromanipulator on (1 1 1) Silicon Substrate," Sens. Actuators, A, **125**(2), pp. 438–445.
[105] Beyeler, F., Neild, A., Oberti, S., Bell, D. J., and Sun, Y., 2007, "Monolithically Fabricated Microgripper With Integrated Force Sensor for Manipulating Microobjects and Biological Cells Aligned in an Ultrasonic field," J. Microelectromech. Syst., **16**(1), pp. 7–15.
[106] Qiao, D.-Y., Yuan, W.-Z., and Li, X.-Y., 2007, "A Two-Beam Method for Extending the Working Range of Electrostatic Parallel-Plate Micro-Actuators," J. Electrost., **65**(4), pp. 256–262.
[107] Hung, E. S., and Senturia, S. D., 1999, "Extending the Travel Range of Analog-Tuned Electrostatic Actuators," J. Microelectromech. Syst., **8**(4), pp. 497–505.
[108] Chan, E. K., and Dutton, R. W., 2000, "Electrostatic Micromechanical Actuator With Extended Range of Travel," J. Microelectromech. Syst., **9**(3), pp. 321–328.

[109] Castañer, L., Pons, J., Nadal-Guardia, R., and Rodríguez, A., 2001, "Analysis of the Extended Operation Range of Electrostatic Actuators by Current-Pulse Drive," Sens. Actuators, A, **90**(3), pp. 181–190.
[110] Rocha, L. A., Cretu, E., and Wolffenbuttel, R. F., 2006, "Using Dynamic Voltage Drive in a Parallel-Plate Electrostatic Actuator for Full-Gap Travel Range and Positioning," J. Microelectromech. Syst., **15**(1), pp. 69–83.
[111] Li, L., Brown, J. G., and Uttamchandani, D., 2002, "Study of Scratch Drive Actuator Force Characteristics," J. Micromech. Microeng., **12**(6), pp. 736–741.
[112] Kanamori, Y., Yahagi, H., and Hane, K., 2006, "A Microtranslation Table With Scratch-Drive Atuators Fabricated From Silicon-on-Insulator Wafer," Sens. Actuators, A, **125**(2), pp. 451–457.
[113] Kuang, Y., Huang, Q. A., and Lee, N. K. S., 2002, "Numerical Simulation of a Polysilicon Thermal Flexure Actuator," Microsyst. Technol., **8**(1), pp. 17–21.
[114] Li, R., Huang, Q.-A., and Li, W., 2009, "A Nodal Analysis Model for the Out-of-Plane Beamshape Electrothermal Microactuator," Microsyst. Technol., **15**(2), pp. 217–225.
[115] Enikov, E. T., Kedar, S. S., and Lazarov, K. V., 2005, "Analytical Model for Analysis and Design of V-Shaped Thermal Microactuators," J. Microelectromech. Syst., **14**(4), pp. 788–798.
[116] Lin, L., and Chiao, M., 1996, "Electrothermal Responses of Lineshape Microstructures," Sens. Actuators, A, **55**(1), pp. 35–41.
[117] Mayyas, M., and Stephanou, H., 2009, "Electrothermoelastic Modeling of MEMS Gripper," Microsyst. Technol., **15**(4), pp. 637–646.
[118] Hickey, R., Sameoto, D., Hubbard, T., and Kujath, M., 2003, "Time and Frequency Response of Two-Arm Micromachined Thermal Actuators," J. Micromech. Microeng., **13**(1), pp. 40–46.
[119] Geisberger, A. A., Sarkar, N., Ellis, M., and Skidmore, G. D., 2003, "Electrothermal Properties and Modeling of Polysilicon Microthermal Actuators," J. Microelectromech. Syst., **12**(4), pp. 513–523.
[120] Liu, C., 2006, *Foundations of MEMS*, Pearson/Prentice-Hall, Upper Saddle River, NJ.
[121] Atre, A., 2007, "Effect of Shape Factors and Material Property Variations on Modeling the Response of Thermal Microactuators," Sens. Actuators, A, **134**(1), pp. 69–76.
[122] Mankame, N. D., and Ananthasuresh, G. K., 2001, "Comprehensive Thermal Modelling and Characterization of an Electro-Thermal-Compliant Microactuator," J. Micromech. Microeng., **11**(5), pp. 452–462.
[123] Mills, A., 1999, *Basic Heat and Mass Transfer*, Prentice-Hall, Englewood Cliffs, NJ.
[124] Atre, A., and Boedo, S., 2004, "Effect of Thermophysical Property Variations on Surface Micromachined Polysilicon Beam Flexure Actuators," Proceedings of the Modeling and Simulation of Microsystems, NSTI-Nanotech 2004, Vol. 2, pp. 263–267.
[125] Sundararajan, S., and Bhushan, B., 2002, "Development of AFM-based Techniques to Measure Mechanical Properties of Nanoscale Structures," Sens. Actuators, A, **101**(3), pp. 338–351.
[126] Godoy, P. H. D., and Silva, E. C. N., 2007, "Aspects of Fabrication and Characterization of Electro-Thermal Microactuators," J. Braz. Soc. Mech. Sci., **29**(1), pp. 26–33.
[127] Lee, K. B., Pisano, A. P., and Lin, L., 2007, "Nonlinear Behaviors of a Comb Drive Actuator Under Electrically Induced Tensile and Compressive Stresses," J. Micromech. Microeng., **17**(3), pp. 557–566.
[128] Leus, V., and Elata, D., 2004, "Fringing Field Effect in Electrostatic Actuators," Technion-Israel Institute of Technology Technical Report No. ETR-2004-2.
[129] Zhu, G., Penet, J., and Saydy, L., 2007, "Modeling and Control of Electrostatically Actuated MEMS in the Presence of Parasitics and Parametric Uncertainties," ASME J. Dyn. Syst., Meas., Control, **129**(6), pp. 786–794.
[130] Elata, D., and Bamberger, H., 2006, "On the Dynamic Pull-in of Electrostatic Actuators With Multiple Degrees of Freedom and Multiple Voltage Sources," J. Microelectromech. Syst., **15**(1), pp. 131–140.
[131] Lin, W.-H., and Zhao, Y.-P., 2005, "Nonlinear Behavior for Nanoscale Electrostatic Actuators With Casimir Force," Chaos, Solitons Fractals, **23**(5), pp. 1777–1785.
[132] Qinghua, L., Yanbin, F., and Xianmin, Z., 2008, "In-Plane Micro-Motion Measurement With High Accuracy Based on Computer Microvision," Seventh World Congress on Intelligent Control and Automation, WCICA 2008, pp. 2365–2370.
[133] Zhong, Y., Zhang, G., Leng, C., and Zhang, T., 2007, "A Differential Laser Doppler System for One-Dimensional In-Plane Motion Measurement of MEMS," Measurement, **40**(6), pp. 623–627.
[134] Park, H., Kwon, S., and Kim, S., 2009, "Quantitative Displacement Measurement of a Nanotube Cantilever With Nanometer Accuracy Using Epifluorescence Microscopy," Rev. Sci. Instrum., **80**(5), p. 053703.
[135] Lai, Y., Mcdonald, J., Kujath, M., and Hubbard, T., 2004, "Force, Deflection and Power Measurements of Toggled Microthermal Actuators," J. Micromech. Microeng., **14**(1), pp. 49–56.
[136] Sun, Y., and Nelson, B. J., 2007, "MEMS Capacitive Force Sensors for Cellular and Flight Biomechanics," Biomed. Mater., **2**(1), pp. S16–S22.
[137] Wittwer, J. W., Baker, M. S., and Howell, L. L., 2006, "Simulation, Measurement, and Asymmetric Buckling of Thermal Microactuators," Sens. Actuators, A, **128**(2), pp. 395–401.
[138] Tokunaga, M., Aoki, T., Hiroshima, M., Kitamura, K., and Yanagida, T., 1997, "Subpiconewton Intermolecular Force Microscopy," Biochem. Biophys. Res. Commun., **231**(3), pp. 566–569.
[139] Teyssieux, D., Thiery, L., and Cretin, B., 2007, "Near-Infrared Thermography Using a Charge-Coupled Device Camera: Application to Microsystems," Rev. Sci. Instrum., **78**(3), p. 034902.
[140] Kim, S. H., Noh, J., Jeon, M. K., Kim, K. W., Lee, L. P., and Woo, S. I., 2006, "Micro-Raman Thermometry for Measuring the Temperature Distribution Inside the Microchannel of a Polymerase Chain Reaction Chip," J. Micromech. Microeng., **16**(3), pp. 526–530.
[141] Serrano, J. R., and Kearney, S. P., 2008, "Time-Resolved Micro-Raman Thermometry for Microsystems in Motion," ASME J. Heat Transfer, **130**(12), p. 122401.
[142] Jalili, N., and Laxminarayana, K., 2004, "A Review of Atomic Force Microscopy Imaging Systems: Application to Molecular Metrology and Biological Sciences," Mechatronics, **14**(8), pp. 907–945.
[143] Madou, M. J., 2002, *Fundamentals of Microfabrication: The Science of Miniaturization*, CRC, Boca Raton, FL.
[144] Judy, J. W., 2001, "Microelectromechanical Systems (MEMS): Fabrication, Design and Applications," Smart Mater. Struct., **10**(6), pp. 1115–1134.
[145] Gad-El-Hak, M., 2006, *MEMS: Introduction and Fundamentals*, CRC, Boca Raton, FL/Taylor & Francis, New York.
[146] Maleville, C., and Mazuré, C., 2004, "Smart-Cut® Technology: From 300 mm Ultrathin SOI Production to Advanced Engineered Substrates," Solid-State Electron., **48**(6), pp. 1055–1063.
[147] Chen, Y., and Pépin, A., 2001, "Nanofabrication: Conventional and Nonconventional Methods," Electrophoresis, **22**(2), pp. 187–207.
[148] Morton, K. J., Nieberg, G., Bai, S., and Chou, S. Y., 2008, "Wafer-Scale Patterning of Sub-40 nm Diameter and High Aspect Ratio (>50:1) Silicon Pillar Arrays by Nanoimprint and Etching," Nanotechnology, **19**(34), p. 345301.
[149] Shedd, G. M., and Russell, P., 1990, "The Scanning Tunneling Microscope as a Tool for Nanofabrication," Nanotechnology, **1**(1), pp. 67–80.
[150] Binnig, G., Quate, C. F., and Gerber, C., 1986, "Atomic Force Microscope," Phys. Rev. Lett., **56**(9), pp. 930–933.
[151] Huo, F., Zheng, Z., Zheng, G., Giam, L. R., Zhang, H., and Mirkin, C. A., 2008, "Polymer Pen Lithography," Science, **321**, pp. 1658–1660.
[152] Cheng, C.-H., Chan, C.-K., and Lai, G.-J., 2009, "Optimal Design of Al/Si Bimorph Electro-Thermal Microactuator by Integrating Finite-Element Code With Optimization Method," Sens. Actuators, A, **151**(1), pp. 53–63.
[153] Choi, H.-S., Lee, D.-C., Kim, S.-S., and Han, C.-S., 2005, "The Development of a Microgripper With a Perturbation-Based Configuration Design Method," J. Micromech. Microeng., **15**(6), pp. 1327–1333.
[154] Wang, N. F., and Tai, K., 2008, "Design of Grip-and-Move Manipulators Using Symmetric Path Generating Compliant Mechanisms," ASME J. Mech. Des., **130**(11), p. 112305.
[155] Sigmund, O., 2009, "Manufacturing Tolerant Topology Optimization," Acta Mech. Sin., **25**(2), pp. 227–239.
[156] Maute, K., and Frangopol, D. M., 2003, "Reliability-Based Design of MEMS Mechanisms by Topology Optimization," Comput. Struct., **81**(8–11), pp. 813–824.
[157] Du, Y.-X., Chen, L.-P., Tian, Q.-H., and Wu, Z.-J., 2009, "Topology Synthesis of Thermomechanical Compliant Mechanisms With Geometrical Nonlinearities Using Meshless Method," Adv. Eng. Software, **40**(5), pp. 315–322.
[158] van West, E., Yamamoto, A., and Higuchi, T., 2007, "The Concept of "Haptic Tweezer," a Non-Contact Object Handling System Using Levitation Techniques and Haptics," Mechatronics, **17**(7), pp. 345–356.
[159] Lyons, K., and Postek, M., 2008, "Metrology at the Nanoscale: What Are the Grand Challenges?," Proc. SPIE, **7042**, pp. 704202.1–704202.13.